Biochimica et Biophysica Acta 1817 (2012) 44–65

Contents lists available at ScienceDirect

Biochimica et Biophysica Acta

journal homepage: www.elsevier.com/locate/bbabio

Review

# Light-induced quinone reduction in photosystem II ☆

Frank Müh [a,b], Carina Glöckner [a], Julia Hellmich [a], Athina Zouni [a,*]

[a] Max-Volmer-Laboratorium für Biophysikalische Chemie, Technische Universität Berlin, Strasse des 17. Juni 135, D-10623 Berlin, Germany
[b] Institut für Theoretische Physik, Johannes Kepler Universität Linz, Altenberger Strasse 69, A-4040 Linz, Austria

ARTICLE INFO

*Article history:*
Received 14 March 2011
Received in revised form 20 May 2011
Accepted 23 May 2011
Available online 1 June 2011

*Keywords:*
Bicarbonate
Cytochrome *b*559
Lipids
Non-heme iron
Photoinhibition
Reaction center

ABSTRACT

The photosystem II core complex is the water:plastoquinone oxidoreductase of oxygenic photosynthesis situated in the thylakoid membrane of cyanobacteria, algae and plants. It catalyzes the light-induced transfer of electrons from water to plastoquinone accompanied by the net transport of protons from the cytoplasm (stroma) to the lumen, the production of molecular oxygen and the release of plastoquinol into the membrane phase. In this review, we outline our present knowledge about the "acceptor side" of the photosystem II core complex covering the reaction center with focus on the primary ($Q_A$) and secondary ($Q_B$) quinones situated around the non-heme iron with bound (bi)carbonate and a comparison with the reaction center of purple bacteria. Related topics addressed are quinone diffusion channels for plastoquinone/plastoquinol exchange, the newly discovered third quinone $Q_C$, the relevance of lipids, the interactions of quinones with the still enigmatic cytochrome *b*559 and the role of $Q_A$ in photoinhibition and photoprotection mechanisms. This article is part of a Special Issue entitled: Photosystem II.



## 1. Introduction

In the last decade, our knowledge about the spatial structure of key enzymes participating in the electron transfer (ET) processes of oxygenic photosynthesis (Fig. 1A) has advanced considerably [1–12]. The crystal structures are a prerequisite for a ripe understanding of these enzymes, but as a milestone, they mark the beginning rather than the end of a long way. In the case of photosystem II (PSII), the light-driven water:plastoquinone oxidoreductase that enables cyanobacteria, algae and plants to use just water as electron source [13,14], crystal structures have been obtained with resolutions between 3.8 and 2.9 Å [15], and very recently improved to 1.9 Å resolution [16]. These structures feature a rich variety of details that have to be linked to function, a likewise fascinating and challenging task.

The photosynthetic reaction center (RC) of PSII (PSII-RC) is of type II, i.e., it binds at its "acceptor side" two quinones, $Q_A$ and $Q_B$, that are arranged in a symmetry-related manner around a non-heme iron (Fig. 2A). $Q_B$ is the reductase substrate. This motif is a common property of PSII-RC and the RC of purple bacteria (bRC). The structure of the latter was determined earlier in the groundbreaking work of Michel and Deisenhofer [17–22] for *Blastochloris* (formerly *Rhodopseudomonas*) *viridis* and later by Allen and Feher for *Rhodobacter* (formerly *Rhodopseudomonas*) *sphaeroides* [23–31]. Despite the large homology of PSII-RC and bRC, there are distinctive features. The first and most obvious is, that PSII-RC is linked at its "donor side" to the water oxidizing complex (WOC) catalyzing the cleavage of water (Fig. 2) and being able to store oxidation equivalents in order to connect the one-electron processes in the RC to the four-electron process of forming dioxygen (Fig. 3A). We note that the present review does not contain any detailed information concerning the WOC, which has been given elsewhere [13–15,32–36]. The second is, that PSII-RC is embedded in the PSII core complex (PSIIcc) being composed of at least 20 different protein subunits. Thus, a quinol leaving the $Q_B$ pocket will inevitably experience a different chemical environment than its counterpart in bRC before reaching the membrane phase. Third, the $Q_B$ site is closer to the protein surface in PSII-RC than in bRC because the former lacks the cytoplasmic extension of the latter [22,31]. Finally, the chemical details of cofactors are different (e.g., chlorophyll (Chl) *a* versus bacteriochlorophyll (BChl) *a* or *b*, plastoquinone (PQ) versus ubiquinone (UQ)),

*Abbreviations:* ATP, adenosine triphosphate; BChl, bacteriochlorophyll, BNT, 2-bromo-3-methyl-6-isopropyl-4-nitrophenol; bRC, bacterial reaction center (purple bacteria); βDM, n-dodecyl-β-D-maltoside; Car, β-carotene; Chl *a*, chlorophyll *a*; CL, cardiolipin; CS, charge separation; cyt, cytochrome; DCMU, 3-(3,4-dichlorophenyl)-1,1-dimethylurea; DGDG, digalactosyldiacylglycerol; EET, excitation energy transfer; ELDOR, electron–electron double resonance; ENDOR, electron nuclear double resonance; EPR, electron paramagnetic resonance; ESEEM, electron spin echo envelope modulation; ET, electron transfer; FNR, ferredoxin:$NADP^+$ reductase; FTIR, Fourier transform infrared; HP, high potential; HTG, n-heptyl-β-D-thioglucoside; IP, intermediate potential; LMW, low molecular weight; LP, low potential; MGDG, monogalactosyldiacylglycerol; MQ, menaquinone; NADPH, nicotinamide adenine dinucleotide phosphate; NHI, non-heme iron; PG, phosphatidylglycerol; Pheo, pheophytin; PQ, plastoquinone; $PQH_2$, plastoquinol; PSI, photosystem I; PSIIcc, photosystem II core complex; PT, proton transfer; RC, reaction center; ROS, reactive oxygen species; $S_i$, redox state of the WOC; SOD, superoxidase dismutase; SOO, superoxide oxidase; SOR, superoxide reductase; SQDG, sulfoquinovosyldiacylglycerol; TL, thermoluminescence; TMH, transmembrane helix; UQ, ubiquinone; VLP, very low potential; WOC, water oxidizing complex

☆ This article is part of a Special Issue entitled: Photosystem II.

* Corresponding author. Tel.: +49 30 314 25650; fax: +49 30 31421122.
*E-mail address:* athina.zouni@tu-berlin.de (A. Zouni).

0005-2728/$ – see front matter © 2011 Elsevier B.V. All rights reserved.
doi:10.1016/j.bbabio.2011.05.021

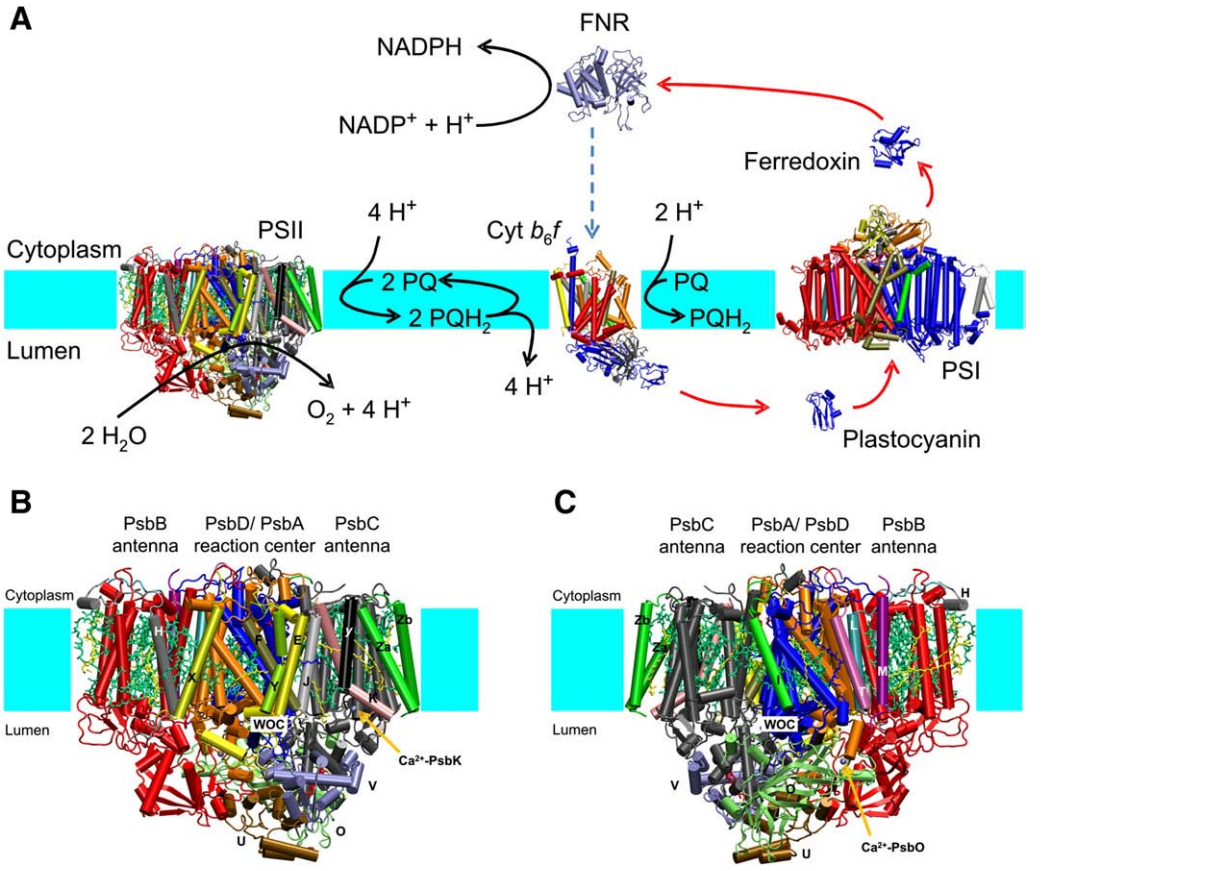


**Fig. 1.** (A) Overview of ET pathways and proton translocation across the thylakoid membrane in oxygenic photosynthesis: PSII from *T. elongatus* (PDB ID: 3BZ1 [11]), cyt $b_6f$ from *C. reinhardtii* (PDB ID: 1Q90 [5]), plastocyanin from *Synechococcus* sp. PCC 7942 (PDB ID: 1BXV [43]), PSI from *T. elongatus* (PDB ID: 1JB0 [1]), ferredoxin from *T. elongatus* (PDB ID: 1CJN [47]), and FNR from *Anabaena* PCC 7119 (PDB ID: 1QUE [49]). For simplicity, only monomers are shown as backbone cartoons with distinct colors for different protein subunits. (B) Structure of one PSIIcc monomer at 2.9 Å resolution [11] viewed along the membrane plane. Small subunits are labeled according to their one-letter code. Small membrane-intrinsic subunits visible are PsbE and F (cyt *b*559) as well as PsbH, J, K, X, Y, and Z. Za, Zb refer to the two TMH of PsbZ. Chl *a* (green) and Car (yellow) pigments are shown as stick models. The positions of the WOC and a $Ca^{2+}$ ion bound to PsbK are indicated. (C) Same as in B, but viewed from the opposite side. The visible small membrane-intrinsic subunits are PsbI, L, M, T, Z and the N-terminus of PsbH. The positions of the WOC and a $Ca^{2+}$ ion bound to PsbO are indicated. Crystal structures were visualized with VMD [354].

which is a consequence of adaption to different light conditions and required redox potentials.

In this review, we outline our present knowledge of the light-dependent quinone reductase activity of PSIIcc based on the 2.9 Å resolution crystal structure [11] (see Section 10 for information regarding the 1.9 Å resolution structure [16]) along with a comparison to bRC (mainly *R. sphaeroides*). The review also covers other aspects of the acceptor side such as the role of integral lipids, cytochrome (cyt) *b559* and the role of quinones in photoinhibition.

## 2. Location and overall structure of photosystem II

### 2.1. Thylakoid membrane and photosynthetic membrane proteins

The biochemical processes of photosynthesis can be devided into two groups: the light reactions, in which solar energy is used to synthesize the cellular energy currency adenosine triphosphate (ATP) and to bind electrons and protons in the form of reduced nicotinamide adenine dinucleotide phosphate (NADPH), and the dark reactions, in which carbon dioxide ($CO_2$) is fixed and converted to carbohydrates under consumption of ATP and NADPH [37–39]. The majority of light reactions is catalyzed by protein complexes harbored in the thylakoid membrane (Fig. 1A). PSII utilizes the electrons taken from water to reduce plastoquinone (PQ) to plastoquinol ($PQH_2$), which diffuses into the membrane and is replaced by fresh PQ. The PQ and $PQH_2$ molecules accumulated in the thylakoid membrane are referred to as quinone pool [40]. $PQH_2$ becomes reoxidized at the cyt $b_6f$ complex [4,5,41,42], which transfers the electrons to the water-soluble carrier plastocyanin (PC), a copper-binding protein [43] (or cyt $c_6$, a heme protein [44]) at the lumenal side of the membrane. PC delivers the electrons to photosystem I (PSI), a light-driven plastocyanin:ferredoxin oxidoreductase [45], which is composed of 12 different polypeptides and binds, among other cofactors, three iron–sulfur clusters of the [4Fe–4S] type in its ET system [1,46]. PSI reduces the soluble [2Fe–2S] protein ferredoxin [47] (or flavodoxin) at the cytoplasmic side of the membrane [48], which in turn supplies the soluble flavoprotein ferredoxin:$NADP^+$ reductase (FNR [49,50]) with electrons for NADPH formation [51]. The combined activity of the membrane proteins involved in this reaction sequence results in a net transport of protons from the cytoplasmic to the lumenal side of the membrane (Fig. 1A), creating an electrochemical potential difference, which is used by the $F_0F_1$-ATP synthase (not shown) for the formation of ATP [52–56].

### 2.2. Protein subunits and cofactors of photosystem II

PSII from the cyanobacterium *Thermosynechococcus elongatus* can be isolated as a monomeric or a dimeric PSIIcc, which both are active in light-induced water oxidation [57,58]. The first crystals of active PSIIcc have been obtained from the dimeric form [59] and allowed to determine the 3D-structure to 3.8 Å resolution [6]. The structure could be refined to a resolution of 2.9 Å [11,15]. Recently, crystallization of the monomeric form could be accomplished, and a first structure at 3.6 Å resolution was determined [12]. Crystallization of dimeric PSIIcc was

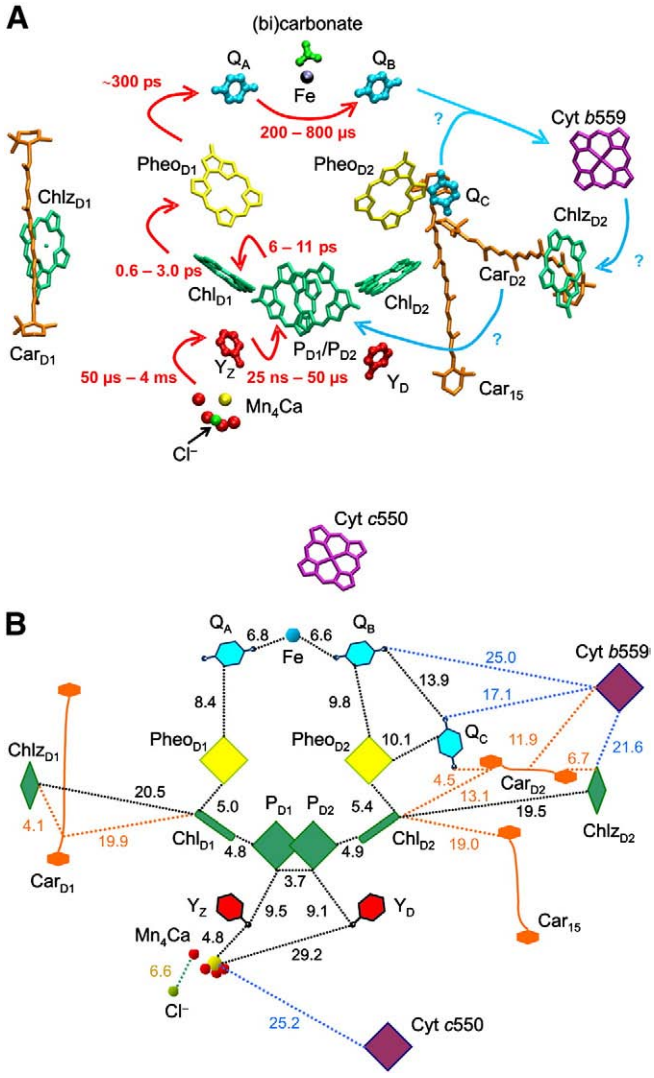


**Fig. 2.** Arrangement of cofactors in and around the RC of PSIIcc according to the 2.9 Å resolution structure [11]. Red arrows indicate ET steps along with their transfer time, detailing the rough scheme in Fig. 3A. Blue arrows denote possible side-path ET processes. Figure made with VMD [354]. (B) Schematic representation of the cofactor arrangement in (A) along with edge-to-edge distances given in Å.

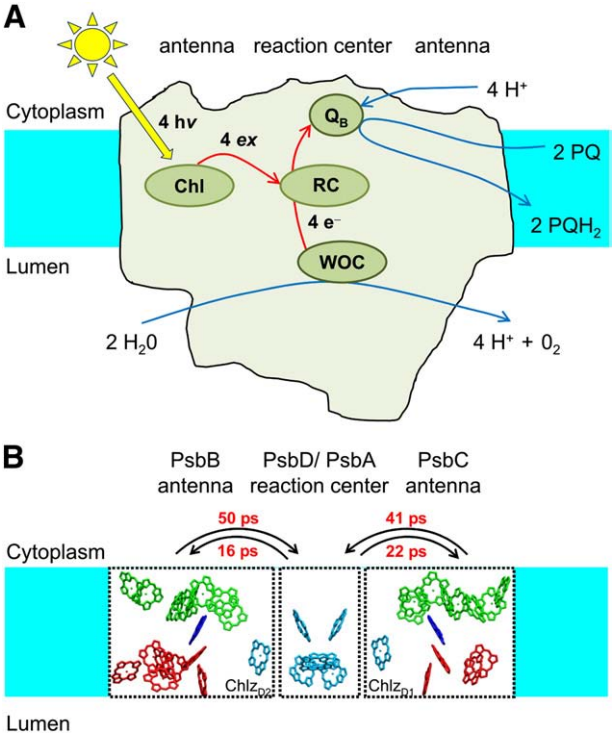


**Fig. 3.** (A) Schematic presentation of ET in PSIIcc (light green) embedded in the thylakoid membrane (blue). Excitation by sunlight (4 hν) (or EET from outer antennae) creates quanta of excitation energy (4 ex) in the Chl of the core antenna system. The excitons are transferred to the RC, where they initiate charge separation and electron (4 $e^-$) transfer. At the "acceptor side" of the RC, the electrons are taken up by the PQ substrate in the $Q_B$ pocket to form $PQH_2$. At the "donor side", electrons are extracted from the WOC. In total, two $PQH_2$ are formed per one $O_2$. Water oxidation and quinone reduction result in the net transport of 4 $H^+$ per $O_2$ from the cytoplasm to the lumen. (B) Arrangement of chlorin pigments in PSIIcc and time constants of EET between the core antennae and RC in a simplified "three-compartment model" based on simulations by Raszewski and Renger [82].

also performed with the cyanobacterium *T. vulcanus*, resulting in a 3.7 Å resolution structure [7], and the red algae *Cyanidium caldarium*, where the structure eludication is still at an early stage [60]. Very recently, crystallization of dimeric PSIIcc from higher plants (*Nicotiana tabacum*) was accomplished with crystals diffracting up to 7.0 Å resolution [61], and a crystal structure of dimeric PSIIcc from *T. vulcanus* with a resolution of 1.9 Å was published [16].

Each PSIIcc-monomer consists of at least 20 different polypeptide chains, with the majority of subunits (17) being membrane-spanning and α-helical (Fig. 1B, C) [62]. Two of these intrinsic subunits, PsbA (D1) and PsbD (D2) with five transmembrane helices (TMH) each, form the RC of PSIIcc harboring most redox-active cofactors. The PSII-RC is structurally homologous to bRC [21,22,31,63] and thus contains two symmetry-related branches of cofactors (Fig. 2): The two closely interacting Chl *a*, $P_{D1}$ and $P_{D2}$, the two Chl *a*, $Chl_{D1}$ and $Chl_{D2}$, two pheophytins *a*, $Pheo_{D1}$ and $Pheo_{D2}$, as well as two PQ, $Q_A$ and $Q_B$. Situated between $Q_A$ and $Q_B$ is a non-heme iron, to which a (bi) carbonate anion is ligated. In addition, there are two Chl *a* in the periphery of the RC, $Chlz_{D1}$ and $Chlz_{D2}$. The 2.9 Å structure [11] also revealed a third PQ ($Q_C$) being present in the crystallized dimeric PSIIcc.

Following the approximate $C_2$-symmetry of the RC, the two subunits PsbB (CP47) and PsbC (CP43), each with six TMHs, bind 16 and 13 Chl *a*, respectively, serving as light-harvesting pigments that transfer excitation energy to the RC (Fig. 3) [62]. In the 2.9 Å resolution crystal structure all 35 Chl *a* could be completely modeled for the first time. Besides their role as antenna proteins PsbB and PsbC, with their large membrane extrinsic loops at the lumenal side, are important for assembly and stabilization of the whole PSIIcc and the WOC [13,16,64–66].

Carotenoids fulfill a number of functions in photosynthetic proteins [67,68] including light-harvesting, regulation of excitation energy transfer (EET) [69], quenching of Chl triplet states, scavenging of singlet oxygen, ET [70] and structure stabilization. There are 12 β-carotene (Car) molecules per monomeric PSIIcc, one ($Car_{15}$) being only found at 2.9 Å resolution [11]. The particular roles of the Cars in PSIIcc still have to be elucidated, but most of them likely serve as light-harvesting pigments or triplet quenchers and help to stabilize the PSIIcc structure [71].

PSIIcc has a high content of integral lipids. Besides the 14 lipid molecules modeled for the first time at 3.0 Å resolution [10], eleven new lipids were found at 2.9 Å [11]. The lipid composition of PSIIcc roughly reflects that of the thylakoid membrane [72], but the distribution is asymmetric. The head groups of negatively charged phosphatidylglycerol (PG) and sulfoquinovosyldiacylglycerol (SQDG) are exclusively located at the cytoplasmic side, those of uncharged digalactosyldiacylglycerol (DGDG) at the lumenal side and those of monogalactosyldiacylglycerol (MGDG) at both sides. In addition,

seven detergent molecules n-dodecyl-β-D-maltoside (βDM) per monomer could be identified which may have replaced galactolipids (DGDG or MGDG) during the isolation procedure, because of their similar sugar head groups. It is thus possible that there are even more integral lipids bound to native PSIIcc (see also Section 10). The most remarkable structural feature is a cluster of eight lipid molecules (containing all types of lipids), which forms a shallow isolated bilayer within PSIIcc [11,15]. In the monomeric PSIIcc crystal structure, the lipid inventory was found to be essentially the same as that of the PSIIcc dimer. The lipid bilayer at the PQ/$PQH_2$ exchange cavity found in the PSIIcc dimer was also observed in the monomer, but lacking one MGDG molecule. Therefore, the possible shielding function of MGDG is missing and the $Q_B$ pocket might be more accessible for molecules from the aqueous phase, explaining the substitution of $Q_B$ with a buffer molecule in the monomeric PSIIcc structure [12].

The remaining membrane-intrinsic subunits of PSIIcc are small and have only one or two TMH. Structure and function of these low molecular weight (LMW) peptides have been reviewed [62,73,74]. Of particular interest from the structural point of view is the three-helix bundle formed by PsbL, PsbM and PsbT at the monomer–monomer interface of the PSIIcc dimer. A genetic deletion of PsbM (the sole direct protein–protein contact between the monomers) in cyanobacteria resulted in a somewhat reduced abundance of PSIIcc dimers, but dimers are still formed [75,76]. Thus, PsbM does not entirely determine dimer formation of PSIIcc and other contacts between the monomers contribute to stabilize the dimer, probably mediated by lipids. However, deletion of both, PsbM and PsbT, results in complete prevention of dimer formation, while strains lacking PsbL assemble neither complete dimers nor monomers [75].

Besides $Mg^{2+}$ (part of Chl *a*) and the four Mn and one $Ca^{2+}$ ions of the WOC, there are other metals bound to PSIIcc. According to the 2.9 Å resolution crystal structure [11], two additional calcium binding sites exist. One is located at the characteristic hook-shaped N-terminal part of PsbK ($Ca^{2+}$-PsbK, Fig. 1B), and the other resides on top of the β-barrel-like structure of PsbO ($Ca^{2+}$-PsbO, Fig. 1C). Both $Ca^{2+}$ ions likely serve to stabilize the protein structure. The remaining important metal of PSIIcc is iron. It occurs in the form of one non-heme iron (Fig. 2, Subsection 4.1) and the two hemes of cyt *b*559 (bound to PsbE/PsbF) and cyt *c*550 (in the extrinsic subunit PsbV; see Figs. 1 and 2). The latter heme is absent in green algae and plants [77,78], and its function in cyanobacterial PSIIcc is presently unknown. Cyt *b*559 is further discussed in Section 7.

## 3. Excitation energy transfer and charge separation

### 3.1. Excitation energy transfer

The properties of light-absorbing pigments in natural photosynthetic systems are modulated by their protein environment in such a way as to enable them to either promote EET, in which only excitation energy but no matter is transported, or ET, in which electrons are shifted and the pigments change their redox state. The latter process takes place in the RC involving a small number of specialized pigments. The number of pigments performing EET is significantly larger so that they can effectively "harvest" photons in order to deliver them to the RC (light-harvesting or antenna pigments). Besides the antenna Chl bound to PsbB and PsbC in PSIIcc, there are additional light-harvesting proteins associated with PSII, the amount of which relative to the core complex can be varied in response to changes in the light conditions and which differ in structure and location between types of organisms [79,80].

Whereas EET from the outer antennae to the core complex is fast (at least in plants, where it occurs in the sub 10 ps time range [14,81]), EET within PSIIcc from the antenna Chl to the RC is slower taking about 40–50 ps (Fig. 3B) [14,62,82,83]. The reason for this delay is the relatively large distance between antenna Chl and RC in PSIIcc. Since charge separation in the RC is again fast, the transfer of excitation energy to the RC is the rate-limiting step for the "trapping" of energy in PSIIcc. We note that there is still some debate on this issue [62,84,85]. The excited state formed in the RC, P*, is predominantly localized on $Chl_{D1}$ at cryogenic temperatures, but distributed to a certain extent over all six chlorin pigments under physiological conditions [14,83]. In contrast, the lowest excited state P* in bRC is localized on the "special pair" $P_L$–$P_M$ [86], the counterpart of the $P_{D1}$–$P_{D2}$-dimer, because of strong wavefunction overlap between the two BChl and a resulting coupling of the excited state to charge-transfer (CT) states [87].

### 3.2. Charge separation

The various experimental and theoretical evidences supporting our current view of charge separation (CS) in PSII-RC have been reviewed very recently [14,83,88], so that we shall give only a brief sketch here: Since the first excited state of the RC is strongly localized on $Chl_{D1}$, it is assumed that CS starts from this pigment by transfer of an electron to $Pheo_{D1}$ in 0.6–3.0 ps (Fig. 2A). The second radical pair, $P_{D1}^{\bullet+}Pheo_{D1}^{\bullet-}$, is formed in 6–11 ps, where $P_{D1}^{\bullet+}$ is the strong oxidant needed for water oxidation. CS is stabilized in the third step by formation of $P_{D1}^{\bullet+}Q_A^{\bullet-}$ in about 300 ps (Subsection 4.2). This mechanism of primary CS is in contrast to that of bRC, where the $P_L$–$P_M$-dimer is the primary electron donor and $B_A$, the counterpart of $Chl_{D1}$, is the primary electron acceptor [86]. However, there is a discussion about the validity of the CS mechanism. Experiments using single-molecule spectroscopy suggest that protein-bound chromophores occur with a distribution of electronic energy levels [89]. Thus, if the distribution is wider than the energy differences between states, multiple pathways of EET or CS can principally be operative. It has been proposed that actually two different CS mechanisms are possible in PSII-RC [90]: One follows the path $Chl_{D1}^{\bullet+}Pheo_{D1}^{\bullet-} \rightarrow P_{D1}^{\bullet+}Pheo_{D1}^{\bullet-}$ and the other the path $P_{D1}^{\bullet+}Chl_{D1}^{\bullet-} \rightarrow P_{D1}^{\bullet+}Pheo_{D1}^{\bullet-}$, so that $P_{D1}$ and $Pheo_{D1}$ are always electron donor and acceptor, respectively, but $Chl_{D1}$ can act as both. Another problem is the experimental finding that CS and ET leading to water oxidation can be induced with photons of wavelengths as long as 800 nm, suggesting the presence of extremely low-lying excited states of PSII-RC [91–93]. At present, nature and function of these "red Chl" in PSIIcc are unknown.

## 4. The iron–quinone acceptor complex

### 4.1. Non-heme iron and bicarbonate

A characteristic feature of type-II RC is the presence of a non-heme iron (NHI) at the acceptor side. This metal center is a hexacoordinate $Fe^{II}$ with a distorted octahedral geometry. Four vertices of the octahedron are occupied by the $N_\varepsilon$-atoms of histidyl ligands, two from each of the two major subunits constituting the RC (Fig. 4). One of the histidines on each side is engaged in hydrogen bonding with the respective quinone. The remaining two ligand positions are taken over by the oxygen atoms of a bidentate ligand, which is bicarbonate (or carbonate, see below) in PSII-RC (Fig. 4A) and a glutamate residue of the M-subunit (Glu M234) in the case of bRC (Fig. 4B).

An important property of the NHI site is the redox midpoint potential of the $Fe^{II}/Fe^{III}$ couple, $E_m(Fe^{II}/Fe^{III})$. Earlier work on spinach chloroplasts indicated the presence of a redox active component between $Q_A$ and $Q_B$ with a midpoint potential of 360 mV at pH 7.8 [94]. Later, this component was shown to have a pH-dependent redox potential varying linearly from 450 to 350 mV between pH 6 and 8 [95], and it was identified as the iron of the iron–quinone acceptor complex by means of electron paramagnetic resonance (EPR) and Mössbauer spectroscopy [96]. The pH-dependence of the potential can be explained by electrostatic coupling to a network of protonatable amino acid residues as shown by structure-based calculations [97]. The redox potential of

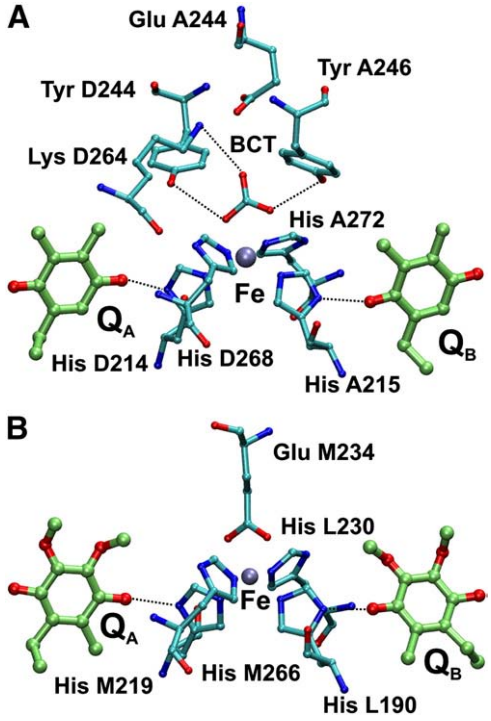


**Fig. 4.** Ligand environment of the NHI (Fe) in (A) PSII-RC of *T. elongatus* (PDB ID: 3BZ1 [11], BCT = bicarbonate) and (B) bRC of *R. sphaeroides* (PDB ID: 2UWU [63]). The dotted lines indicate putative hydrogen bonds. Figures made with VMD [354].

the NHI is too high for a participation in native ET between the quinones. However, it could be demonstrated that exogenous quinones, when brought into the semiquinone form by a normal turnover of the RC (i.e., via $Q_A^{\bullet-}$), can oxidize the iron, which in turn can be re-reduced by $Q_A^{\bullet-}$ [98,99]. Thus, manipulations of the acceptor side can activate redox reactions of the NHI. In contrast, experimental evidence for oxidation of the NHI in bRC has not been reported yet.

Research on the role of bicarbonate in PSIIcc has a long history as reviewed by van Rensen et al. [100]. There is experimental evidence that PSII activity requires bicarbonate: Flushing of samples with nitrogen gas or $CO_2$-depleted air in the presence of high concentrations of formate or acetate results in a significant decrease of ET rates that can be restored to the original values by bicarbonate only. Other bicarbonate-reversible inhibitors are azide, nitrite, nitrate, fluoride [101] or nitric oxide (NO) [102]. Evidence was reported for an influence of bicarbonate on both, the donor and the acceptor side of PSIIcc. Donor side effects will not be further discussed in this review.

The only bicarbonate molecule identified so far in crystallography of PSIIcc is the ligand to the NHI, which is most likely responsible for the acceptor side "bicarbonate effect" [100]. Independent support for the assignment of this ligand comes from earlier spectroscopic work. Petrouleas and Diner [102] provided evidence for ligation of NO to the NHI based on EPR and Mössbauer spectroscopy. The concomitant slowing of ET between $Q_A$ and $Q_B$ is reversed and the characteristic EPR signal of the $Fe^{II}$-NO adduct is diminished by the addition of $NaHCO_3$, indicating that $HCO_3^-$ displaces NO as ligand to the NHI and in this position promotes acceptor side ET [103]. Hienerwadel and Berthomieu [104] performed Fourier transform infrared (FTIR) $Fe^{II}/Fe^{III}$ difference spectroscopy on isotope labeled PSII membranes and concluded that (i) bicarbonate (and not carbonate) is a bidentate ligand to the NHI in the $Fe^{II}$ redox state, (ii) the bicarbonate ligand does not deprotonate upon iron oxidation, but turns into a monodentate ligand, and (iii) a histidyl ligand to the NHI deprotonates upon iron oxidation. The latter process was proposed to determine the pH dependence of $E_m(Fe^{II}/Fe^{III})$. However, the electrostatic computations of Ishikita and Knapp [97] suggest that $pK_a$ shifts of groups outside the first coordination shell of iron can well account for the pH dependence of the redox potential.

The role of the NHI in type-II RC in general is unknown. In the case of PSII-RC, the bicarbonate effect suggests a role of the NHI as regulator of acceptor side ET, although the precise mechanism of this process needs clarification. The physiological role of such a control mechanism has been discussed [105,106] and is related to a down regulation of $O_2$ production in cases of low $CO_2/HCO_3^-$ concentrations to suppress the wasteful reaction of ribulose-1,5-bisphosphate with $O_2$ instead of $CO_2$ (photorespiration [107]). There have been proposals that the NHI might fulfill a protective function against reactive oxygen species (ROS) [106,108]. Indeed, the NHI site of PSIIcc is reminiscent of the active site of superoxide reductase (SOR, catalyzing the reaction $O_2^{\bullet-} + 2H^+ + e^- \rightarrow H_2O_2$), in particular, a nearby Lys residue [109]. It is conceivable that a similar reaction takes place in PSIIcc, if $O_2^{\bullet-}$ displaces the bicarbonate. Superoxide may be formed by side reactions at the acceptor side of PSIIcc as reviewed by Pospíšil [110]. On the other hand, there are structural differences between the NHI sites in SOR and PSII-RC that could allow for different reactions to occur in the latter case. Evidence has been reported for photogeneration of hydroxyl radicals ($OH^{\bullet}$) in PSIIcc with a likely involvement of the NHI [111]. In this case, the NHI would contribute to the formation of ROS rather than to their degradation.

### 4.2. $Q_A$

The primary electron acceptor quinone, $Q_A$, is located between the acceptor pheophytin ($Pheo_{D1}$ or its purple bacterial counterpart $H_A$) and the NHI (Fig. 2), where it functions as one-electron transmitter ultimately delivering electrons for the reduction of the substrate quinone, $Q_B$ (see Section 5). PQ bound to the $Q_A$ site of PSII-RC and UQ bound to the bRC of *R. sphaeroides* are 1,4-benzoquinone derivatives. Other bRC bind menaquinone (MQ), a 1,4-naphthoquinone derivative, in the $Q_A$ site (e.g., *B. viridis* [112,113]). While the quinone molecule as a whole is mainly bound to the protein by van der Waals interaction between the isoprenoid tail and its largely unpolar protein environment, the position of the head group is fixed by two hydrogen bonds and a kind of π-stacking interaction to a Trp residue (Fig. 5). The hydrogen bonds are between the keto oxygens of the quinone and the $N_\delta$-atom of one histidyl ligand to the NHI on one side and to a backbone amide group on the other side (dotted lines in Fig. 5). The π-stacking of PQ or UQ with Trp is in an offset-stacked geometry [114] with a slight tilt of the π-planes against each other. In *B. viridis*, the binding geometry of MQ is similarly offset-stacked, but with parallel π-planes (see, e.g., PDB ID: 1PRC [112]). In all cases, the Trp side chain is stabilized by a hydrogen bond to a Thr residue (D217 in *T. elongatus* and M222 in *R. sphaeroides*, see Fig. 5; M220 in *B. viridis*, not shown).

In bRC of *R. sphaeroides*, the reduction of $Q_A$ by $H_A^{\bullet-}$ occurs in ~200 ps at room temperature [115]. For the corresponding reaction between $Pheo_{D1}^{\bullet-}$ and $Q_A$ in PSII-RC, values between 200 and 500 ps have been reported [116–121]. A difficulty in assigning these numbers is that the formed state $P_{D1}^{\bullet+}Q_A^{\bullet-}$ is subject to energetic relaxation processes and does not attain a true thermodynamic equilibrium during its life time [122,123]. The influence of Trp M252 and Thr M222 in *R. sphaeroides* was studied by employing site-directed mutagenesis [124]. Replacing the former with Tyr or Phe or exchanging the latter to Val causes a destabilization of $Q_A$ in its binding pocket in accordance with the idea that π-stacking with Trp M252 along with a proper orientation of its side chain is important for quinone binding. The time constant of ET from $H_A^{\bullet-}$ to $Q_A$ was found essentially unaffected by the T(M222)V mutant, but increased considerably to 600 and 900 ps, respectively, in W(M252)Y and W(M252)F indicating an important role of Trp M252. Such a role

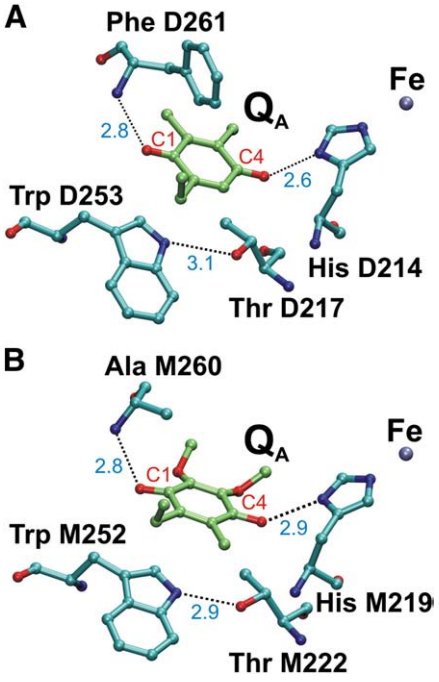


**Fig. 5.** Protein environment of $Q_A$ in (A) PSII-RC of *T. elongatus* (PDB ID: 3BZ1 [11]) and (B) bRC of *R. sphaeroides* (PDB ID: 2UWU [63]). The dotted lines indicate putative hydrogen bonds with distances given in Å. C1 and C4 label the carbonyl carbons of the quinones. Figures made with VMD [354].

was predicted earlier based on quantum chemical calculations [125] suggesting that the electronic coupling between $H_A$ and $Q_A$ is increased due to interaction with the π-system of the Trp side chain (super-exchange coupling). Later molecular dynamics (MD) simulations [126,127] indicated several electron tunneling pathways that may be subject to constructive or destructive interference depending on the protein conformation, so that dynamics is crucial for a deeper understanding of how the protein tunes ET. In the case of PSII-RC, mutagenesis experiments aiming at Trp D253 did not yield a conclusive picture so far. It was merely reported that PSIIcc from the mutant W (D253)L in *Synechocystis* 6803 is highly unstable and it was suggested that this is due to impairment of $Q_A$ binding [128].

In *R. sphaeroides*, the native UQ can be removed from the $Q_A$ pocket [129,130] and the RC can be reconstituted with other quinones having a different redox potential [131,132]. As a consequence, the free energy of the state $P^{\bullet+}Q_A^{\bullet-}$ is varied and its relationship to ET rates can be analyzed. From these experiments, the quantum yield for the formation of $P^{\bullet+}Q_A^{\bullet-}$ was found to exhibit a bell-shaped dependence on the free energy change $\Delta G^0$ for the ET from $H_A^{\bullet-}$ to $Q_A$ and to approach unity for $-\Delta G^0 \approx 600$ meV [133]. This result implies that a significant fraction of the photon energy absorbed by the RC (~1.4 eV) is thermalized in order to stabilize the charge-separated state. Taking into account the additional energy dissipation associated with ET starting from P* (the free energy level of $P^{\bullet+}Q_A^{\bullet-}$ is ~850–900 meV below P* [134–137]) and the energy loss accompanying the further ET to $Q_B$ (~50 meV [138]), only about 33% of the photon energy is retained in the state $P^{\bullet+}Q_B^{\bullet-}$. The formation of $P^{\bullet+}Q_A^{\bullet-}$ is the mostly energy consuming step. A significantly smaller energy loss has been estimated for PSII-RC, where $P_{D1}^{\bullet+}Q_A^{\bullet-}$ is ~300–360 meV below $P_{D1}^{\bullet+}Pheo_{D1}^{\bullet-}$ [139,140]. The value for the free energy difference between P* and $P_{D1}^{\bullet+}Q_A^{\bullet-}$ is ~500 meV [141]. We note that a larger value of 770 meV was given for cyanobacterial PSIIcc [142]. A part of the difference is likely due to Mn-depletion of the used samples. The photon energy is higher (~1.8 eV) in PSII-RC compared to bRC, so that about 70% of this energy is finally stored in the charge-separated state.

Earlier work on bRC resulted in different conclusions concerning a possible pH-dependence of the free energy of $P^{\bullet+}Q_A^{\bullet-}$ and the redox potential $E_m(Q_A/Q_A^{\bullet-})$ [135,143–145]. More recent experiments suggest no or a weak pH-dependence consistent with substoichiometric proton uptake at the acceptor side [136,137,146]. In the case of PSII-RC, the determination of $E_m(Q_A/Q_A^{\bullet-})$ was complicated by the apparent existence of two conformations with strongly different potentials. Based on careful experiments, Krieger et al. [147] assigned a value of $E_m(Q_A/Q_A^{\bullet-}) \approx -80$ mV to intact PSIIcc and $E_m(Q_A/Q_A^{\bullet-}) \approx +65$ mV to samples made inactive in $O_2$-evolution by low-pH treatment. Notably, the potential in both forms is pH-independent between pH 5.5 and 7.5 [147]. Furthermore, Johnson et al. [148] could demonstrate that photoassembly of the WOC shifts $Q_A$ back from the high to the low potential form. These results indicate a conformational connection between donor and acceptor side in PSII-RC. The potential shift of $Q_A$ was suggested to be part of a photoprotection mechanism (Section 8).

Structure-based computations revealed that the $Q_A$ binding pocket is designed to stabilize a negative surplus charge on the quinone in bRC [149]. In particular, several polar residues, including Thr M222 (Fig. 5B), rearrange their hydroxyl dipoles to stabilize the charge. The same was found for the analogous Thr D217 in PSII-RC and was proposed to be related to the observed redox potential shifts of $Q_A$ [150]. Because of their outstanding importance for an understanding of the energetics of protein–cofactor interactions, polar hydrogens, and especially hydrogen bonding interactions of $Q_A$, were in the focus of numerous spectroscopic studies. In this respect, a suitable technique is FTIR spectroscopy. In bRC, bands at 1660 and 1601 $cm^{-1}$ have been assigned to the C═O stretching vibrations at C1 and C4, respectively (Fig. 5B), indicating a significant asymmetry [151,152]. Different numbering schemes for quinones are in use [132]. Here, we use the convention, that C1 is the carbonyl carbon proximal to the isoprenoid chain, for both UQ and PQ. As discussed in greater detail by Wraight and Gunner [132], there is presently no clear explanation for the downshift of the C4═O stretching vibration, but it is not necessarily due to an asymmetry in hydrogen bonding interactions. In the state $Q_A^{\bullet-}$, the C═O bands are no longer independent, but strongly coupled to each other and to C═C modes [132,151,152], making an analysis of specific hydrogen bonding interactions difficult. FTIR spectroscopy was applied to $Q_A$ in PSII-RC prior to the crystal structure elucidation and indicated hydrogen bonding to a His residue analogous to bRC [153].

Analysis of the $Q_A$ site by EPR spectroscopy is complicated by the magnetic interaction between the $Q_A^{\bullet-}$ radical anion and the NHI. The EPR spectrum of the $Q_A^{\bullet-}Fe^{II}$ complex in bRC was analyzed by Butler et al. [154] and is characterized by a broad absorption peak at $g = 1.8$. In PSII-RC, a similar, but not identical, signal is observed peaking at $g = 1.9$ [155,156]. Treatment with formate, which displaces the bicarbonate (Section 4.1), turns the signal into a $g = 1.8$ form nearly identical to its counterpart in bRC [157,158]. The shift to $g = 1.9$ in native PSII-RC was ascribed to an influence of bicarbonate on the first coordination sphere of the NHI [156]. Recently, this signal was reinvestigated and simulated [159]. On the basis of these simulations, it was proposed that the ligand to the NHI is carbonate rather than bicarbonate in contrast to interpretations of FTIR data [104] (Section 4.1).

In bRC, the NHI site can be reconstituted with different metals [160,161]. Also, some bacteria incorporate $Mn^{2+}$ instead of $Fe^{2+}$ under appropriate growth conditions [162]. Of particular interest is the exchange to $Zn^{2+}$, which allows for unperturbed EPR studies of the $Q_A^{\bullet-}$ radical anion [163]. Using EPR and related techniques such as electron nuclear double resonance (ENDOR) and electron spin echo envelope modulation (ESEEM), it could be demonstrated that the hydrogen bonding of $Q_A^{\bullet-}$ is indeed asymmetric with the C4═O carbonyl being more strongly bonded to His M219 than the C1═O to Ala M260 [132]. Another important aspect related to EPR concerns the structural relaxation of $Q_A$ upon reduction. Earlier experiments on the

temperature dependence of ET between the quinones (Section 5) also revealed, that the recombination of the radical pair $P^{\bullet+}Q_A^{\bullet-}$ to the ground state $PQ_A$ is slower in RC frozen under continuous illumination than in RC frozen in the dark, and thus provided direct evidence for conformational changes leading to a stabilization of the charge-separated state [164]. The data were analyzed by assuming a change of the donor–acceptor distance. This could be due to a position shift of either $P^{\bullet+}$ or $Q_A^{\bullet-}$. However, FTIR [151,152] and EPR data [163] argue against a significant change of the position of $Q_A$ at least with respect to the hydrogen bond donors. In addition, time-resolved EPR experiments indicated that the distance between $P^{\bullet+}$ and $Q_A^{\bullet-}$ is not changed upon freezing RC under illumination [165]. The absence of a significant repositioning of $Q_A$ after reduction was confirmed by X-ray crystallography [166,167] and very recently by a combination of ENDOR and electron–electron double resonance (ELDOR) spectroscopy [168].

Several techniques have been applied to uncouple the $Q_A^{\bullet-}$ radical anion from the NHI in PSII-RC: (i) substitution of $Fe^{2+}$ with $Zn^{2+}$ as in bRC [169,170], (ii) iron-depletion by mild trypsin treatment [171], (iii) treatment with $CN^-$ to displace the bicarbonate and change the spin state of the NHI [169,170,172], or (iv) high-pH treatment [173]. An FTIR study was performed on PSII membrane samples treated according to methods (ii)–(iv) and compared with untreated material. It was concluded that the hydrogen bonding interactions of $Q_A^{\bullet-}$ remain virtually unaffected by method (ii), but are drastically changed by the other two methods [174]. Nonetheless, there is a consensus that the hydrogen bonding interaction of $Q_A^{\bullet-}$ is asymmetric, with the C4═O group making a stronger bond to His D214 than the C1═O group to the peptide backbone as in the case of purple bacteria.

### 4.3. $Q_B$

A characteristic of the secondary quinone, $Q_B$, is that it is a substrate and not a tightly bound redox mediator. Consequently, it is more easily lost during sample preparation and can give rise to incomplete occupancy of the $Q_B$ site [22]. Allen et al. [25,28] were the first to report a complete structure of native UQ in bRC from *R. sphaeroides* in a position symmetry-related to $Q_A$, which is nowadays referred to as "proximal" position (Fig. 6B). Later, other bRC structures of *R. sphaeroides* strains were published that showed $Q_B$ in a variety of different positions [162,175–177]. With the aim to clarify the problem of light-induced structural changes [164], Stowell et al. [178] performed X-ray crystallography on RC frozen in the dark and frozen in the light (thus in the state $P^{\bullet+}Q_B^{\bullet-}$). In their "dark structure", UQ is mainly found in a position very similar, but not identical, to that reported by Ermler et al. [177], which is referred to as the "distal" position (see Fig. 6C for a later variant [63]). The "light structure" features $Q_B$ in the proximal position. However, this strict correlation between illumination and movement to the proximal position was not confirmed in later studies on *B. viridis* [179,180]. In *R. sphaeroides*, the distribution between the two positions in the dark was shown to depend on temperature and cryoprotectant [181]. A recent study found UQ in a rather balanced distribution between proximal and distal positions in *R. sphaeroides* both in the dark and in the light with a pH-dependent occupancy of the proximal site between 35% and 70% [63]. A comprehensive list of quinone positions in the various PDB structure files of bRC with resolutions ≤2.8 Å is given by Wraight and Gunner [132].

Similarly to bRC, it was not possible to model $Q_B$ in the first three-dimensional crystal structure of PSIIcc [6], but it was readily assigned in later refinements [8,10,11,16] in a position corresponding to the proximal site in bRC (Figs. 2 and 6A). So far, there is no evidence for a distal position being occupied by PQ in PSIIcc. We note that $Q_C$ is located at a different site (Sections 4.4 and 6). It could be demonstrated by studies on PSIIcc-preparations from *T. elongatus* that besides $Q_A$ and $Q_B$ at least one additional functional PQ is present in solubilized and crystallized core complexes [57,182,183].

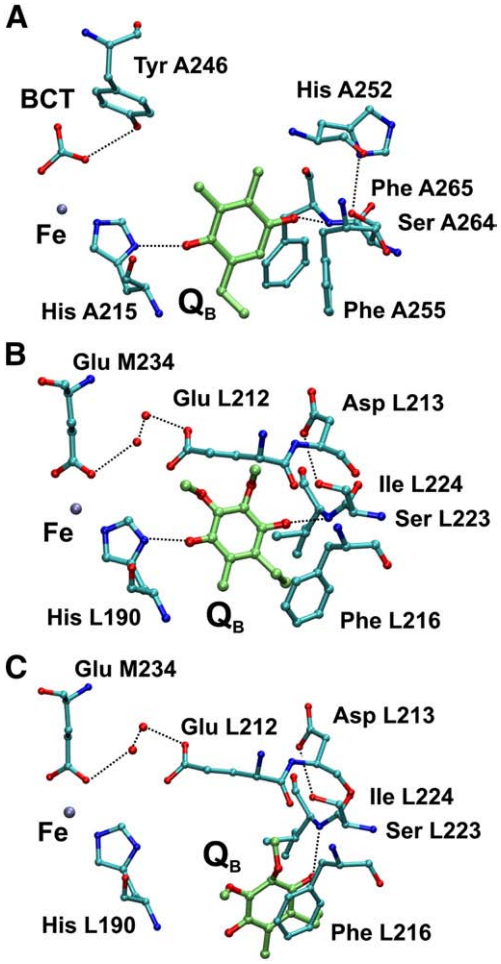


**Fig. 6.** Protein environment of $Q_B$: (A) Position of $Q_B$ in PSII-RC of *T. elongatus* (PDB ID: 3BZ1 [11], BCT = bicarbonate). (B) Proximal position in bRC of *R. sphaeroides* (PDB ID: 2UWU [63]). (C) Distal position in bRC of *R. sphaeroides* [63]. The dotted lines indicate putative hydrogen bonds, and the red spheres represent water molecules. Figures made with VMD [354].

In the proximal position, $Q_B$ forms two hydrogen bonds similar to $Q_A$, one to a histidyl ligand of the NHI (A215 in PSII-RC, L190 in bRC) and the other to the peptide backbone (NH of Phe A265 in PSII-RC, Ile L244 in bRC). A conserved serine residue (A264, L223) is believed to form an additional hydrogen bond after reduction of $Q_B$ (Section 5). In contrast to $Q_A$, $Q_B$ is surrounded by a number of protonatable groups. Glu L212 in bRC is of particular importance for an understanding of proton-coupled ET (Section 5), but is not conserved in PSII-RC (Fig. 6). Another key residue is Asp L213 in bRC, replaced by His A252 in PSII-RC, which is likely involved in proton transfer to $Q_B$. Also, protein-bound water molecules play a role, of which two are shown in Figs. 6B and C (see also Section 10).

In the distal position, the quinone is able to retain its hydrogen bond to the peptide backbone of Ile L224, but the one to the histidyl ligand of the NHI is inevitably broken (Fig. 6C). Instead, there is a π-stacking interaction with the side chain of Phe L216 in an offset-stacked geometry similar to the interaction between $Q_A$ and Trp M252. Support for the idea, that this π-stacking stabilizes the UQ-headgroup, comes from a study on a herbicide-resistant mutant of *B. viridis*, in which Phe L216 is replaced with Ser. The mutation decreases the affinity of bRC for UQ [184]. This result suggests that occupation of the distal position is an important intermediate step in substrate binding to the quinone-reductase part of type-II RC. Indeed, the phenylalanine is conserved in PSII-RC, viz. Phe A255 (Fig. 6A).

In the original work of Stowell et al. [178] the $Q_B$ movement from the distal to the proximal site was accompanied by a 180° propeller twist of the quinone head group. A later analysis based on data with a higher resolution found the electron density of $Q_B$ not well enough defined to decide about such a rotation [185]. A similar problem occurred in the most recent study [63], and the $Q_B$ movement was modeled without the twist (Fig. 6B and C) as supported by simulations.

FTIR spectroscopy applied to the neutral $Q_B$ in bRC was interpreted in terms of a symmetric hydrogen bonding situation consistent with the proximal position [186,187] and unaffected by freezing under illumination [188]. Other authors reported additional evidence for a subpopulation of a more loosely bound UQ without significant hydrogen bonding [189]. The researchers agree, that in the state $Q_B^{\bullet-}$, the quinone remains unprotonated and is symmetrically hydrogen bonded in contrast to $Q_A$ [190]. A more symmetric hydrogen bonding arrangement in $Q_B^{\bullet-}$ compared to $Q_A^{\bullet-}$ is in agreement with ENDOR studies of $Q_B^{\bullet-}$ on $Zn^{2+}$-substituted bRC [163]. Differences in the hydrogen bonding characteristics between $Q_A^{\bullet-}$ and $Q_B^{\bullet-}$ were also found by FTIR in PSII-RC [191].

### 4.4. $Q_C$

Fig. 7A shows the unexpected electron density in the $Q_C$ site found at 2.9 Å resolution in dimeric PSIIcc [11,15] to substantiate its assignment to a PQ molecule. The headgroup of $Q_C$ is located at a distance of ~14 Å from that of $Q_B$ (Fig. 2B). The additional PQ lies in one of the two putative quinone diffusion pathways discussed in Section 6 (Fig. 8). Here, we pose the question of how the headgroup of $Q_C$ is stabilized in order to be well enough defined for a crystallographic detection. The molecule resides in a fairly hydrophobic environment without any obvious polar contact or π-stacking that could stabilize the orientation of the headgroup (Fig. 7B). It is likely held in place mainly by van der Waals interactions with the channel walls surrounding it. Interestingly, both carbonyl oxygens of $Q_C$ are located within a distance of 3.3–3.7 Å from methyl groups (C1═O close to one β-ionylidene ring of $Car_{D2}$, C4═O close to the isoprenoid chain of $Q_B$). This could indicate weakly stabilizing interactions with CH-fragments. In the recent crystallographic study of monomeric PSIIcc [12], electron density was found at exactly the same position, but was not well defined and therefore did not allow for a precise assignment to a quinone headgroup.

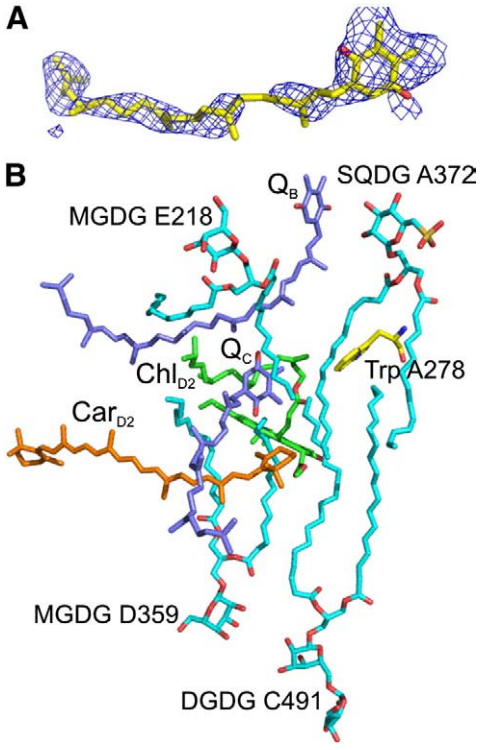


**Fig. 7.** (A) PQ molecule modeled in the $Q_C$ site in PSIIcc of *T. elongatus* at 2.9 Å resolution (PDB ID: 3BZ1 [11]) with electron density (blue mesh) contoured at 1.2σ level. Figure made with PyMOL [355]. (B) Hydrophobic environment of $Q_C$. Figure made with VMD [354].

## 5. Proton-coupled electron transfer between the quinones

### 5.1. First step

The formation of quinol from quinone requires two electrons and two protons and thus needs two turnovers of the RC. The first step is the creation of a semiquinone anion radical $Q_B^{\bullet-}$, which is likely stabilized by protonation of nearby amino acid side chains. Note, that $Q_B$ itself is not protonated in this stage as is evident from spectroscopic studies (Subsection 4.3). It could be shown for bRC that a network of titratable groups (including Glu L212, Asp L213 and Glu M234 shown in Fig. 6) has to take up a proton from the cytoplasm prior to ET, since a negative charge especially around Glu L212 would destabilize the semiquinone state [122,190,192–194]. Some electrostatic computations suggest that the coupling between these residues and $Q_A$ is strong enough so that proton uptake near $Q_B$ could indeed be triggered by the reduction of $Q_A$ [195–198] and adjust the $\Delta G^0$ for ET from $Q_A^{\bullet-}$ to $Q_B$. After arrival of the electron on $Q_B$, further proton uptake and proton rearrangements occur including a proposed orientational switch of the hydroxyl group of Ser L223. Calculations suggest that Ser L223 forms a hydrogen bond to Asp L213 in the state $Q_A^{\bullet-}Q_B$ and to $Q_B^{\bullet-}$ in the state $Q_AQ_B^{\bullet-}$ [122]. This idea is supported by ENDOR spectroscopy [199], but not by FTIR data [190,200]. Whereas Ser L223 is conserved in PSIIcc, Glu L212 and Asp L213 are not (Fig. 6B, C). Structure-based computations suggest that His A252 could take over the role of Asp L213 [150]. However, it is not clear at present, how the absence of an analog of Glu L212 is compensated for in PSII.

In bRC, the ET from $Q_A^{\bullet-}$ to $Q_B$ has the following characteristics: (i) It is heterogeneous and has to be described with at least three time constants of ~10 μs, ~100 μs, and ~1 ms [122]. (ii) It is dependent on the water content of samples [201,202]. (iii) The two larger time constants in (i) are independent of the driving force for ET as shown by substituting quinones with different redox potentials for the native UQ in the $Q_A$ site [203,204]. (iv) The ET rates at cryogenic temperatures differ significantly depending on whether the RC are frozen in the light or in the dark [164]. These results were interpreted in terms of a "gating mechanism": not ET is rate-limiting, but other processes that likely require an activation energy and are triggered by light-induced $Q_A$ reduction. The possible processes discussed to be involved in the gating mechanism are proton transfer and reorganization events as discussed above, protein conformational changes [205,206] and/or a movement of $Q_B$ from the distal to the proximal binding site [178]. Also, the possibility of a redox intermediate between $Q_A$ and $Q_B$ is debated [207–209].

In PSIIcc, the ET from $Q_A^{\bullet-}$ to $Q_B$ is characterized by the following findings: (i) It is heterogeneous and has to be described with at least two time constants of 0.2–0.8 ms and 2–3 ms [210]. (ii) It is influenced by pH [210–212], $H_2O/D_2O$ exchange [210,213,214], and dehydration [215,216] suggesting a coupling to proton transfer and/or water-dependent structural relaxation processes. (iii) It is coupled to protein dynamics and exhibits a marked temperature dependence being completely blocked below 200 K [14,182,216,217]. (iv) The overall reaction is much slower than expected from an analysis of electron tunneling between the quinones, suggesting that ET is not rate-limiting [14,218]. On the basis of these data, it is tempting to consider that a similar gating mechanism is operative in PSIIcc as discussed for bRC.

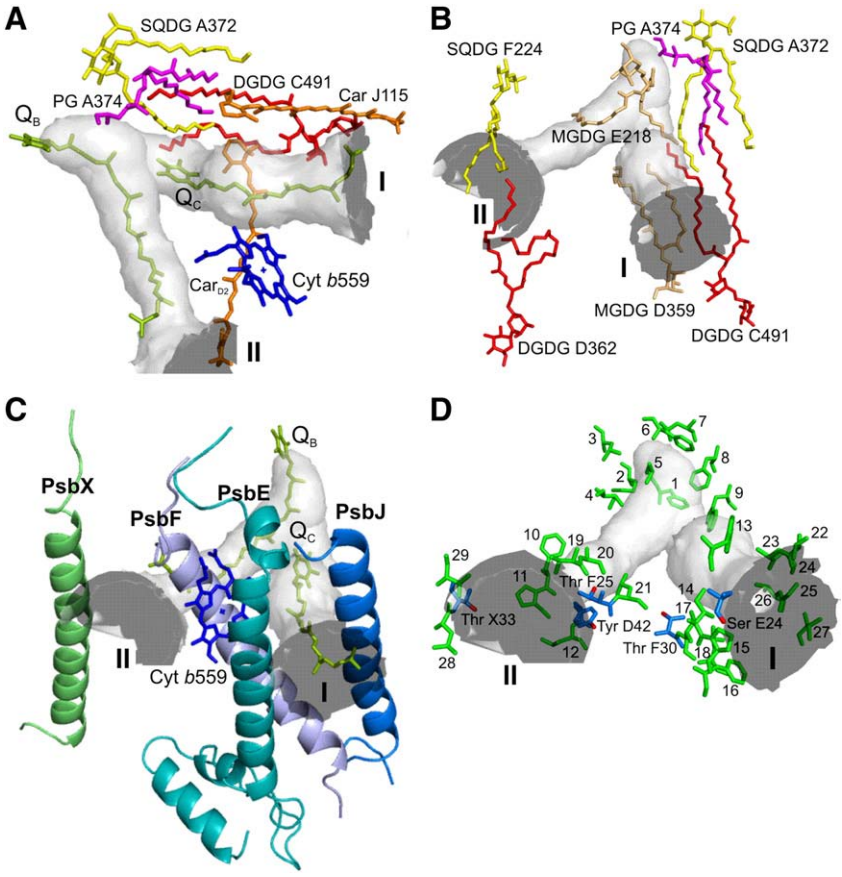


**Fig. 8.** Quinone diffusion channels I and II in PSIIcc of *T. elongatus* identified at 2.9 Å resolution (PDB ID: 3BZ1 [11]) shown as gray boundary surfaces: (A) Location of $Q_B$, $Q_C$, the heme group of cyt *b*559, $Car_{D2}$ (D358), Car J115 and lipids close to the channels. (B) Lipid molecules contributing to the channel walls. (C) Location of the TMH of PsbE and PsbF (constituting cyt *b*559) as well as of PsbJ and PsbX relative to the channel entrances facing the membrane interior. Also shown are $Q_B$, $Q_C$ and the heme group of cyt *b*559. (D) Amino acid residues contributing to the channel walls. Hydrophobic residues are shown in green and polar residues in blue with side chain oxygens in red. The numbering of hydrophobic residues is explained in Table 1. Figures made with PyMOL [355].

### 5.2. Second step

As illustrated in Scheme 1, the second ET to $Q_B$ is coupled to the delivery of the first proton ($H_I^+$).

A key question is whether (i) proton transfer (PT) follows ET (ET/PT mechanism via $Q_AQ_B^{2-}$), (ii) ET follows PT (PT/ET mechanism via $Q_A^{\bullet-}Q_BH$), or (iii) ET and PT occur in a concerted manner (CPET mechanism). This problem was systematically studied by Graige et al. [219–221] for bRC, applying quinone exchange procedures to vary redox potentials and p$K_a$ values. Their data suggest that the PT/ET mechanism is valid [192]. This result is reasonable from the viewpoint of electrostatics, as the highly charged species $Q_AQ_B^{2-}$ constitutes a higher energetic barrier than the intermediate $Q_A^{\bullet-}Q_BH$. Consequently, a similar PT/ET reaction sequence is assumed for PSII-RC [106,222].

In bRC, the first proton ($H_I^+$) is delivered via Ser L223, which takes up a proton from Asp L213 [192]. The second proton ($H_{II}^+$) enters via Glu L212, which is substantiated by the finding that in the mutant E (L212)Q the last step in the reaction sequence of Scheme 1 is blocked [223,224]. By analogy, we can assume that in PSII-RC, the first proton is delivered via His A252 and Ser A264. However, we face the problem that there is no counterpart to Glu L212. Instead, it has been suggested that the (bi)carbonate ligand to the NHI could be involved in proton delivery to $Q_B$ [159,225].

## 6. Lipid-quinone interactions and transport channels

### 6.1. Channel environment

In the course of electron transport, the doubly reduced and doubly protonated mobile carrier $PQH_2$ has to be replaced from the $Q_B$ site by fresh PQ from the quinone pool located in the thylakoid membrane. For the exchange of these hydrophobic molecules, pathways are

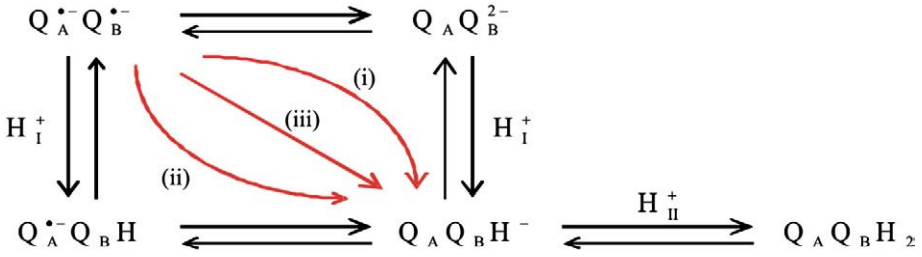


**Scheme 1.** Possible reaction sequences for transport of the second electron and two protons to $Q_B$.

needed which connect the $Q_B$ site with the membrane phase, as the $Q_B$ site is buried inside the PSIIcc. The structural model of *T. elongatus* at 2.9 Å resolution [11] revealed two possible pathways for PQ/$PQH_2$ exchange termed channels I and II. These channels are located in subunit PsbA and converge in the $Q_B$ cavity, which is located close to the cytoplasmic side. The hydrophobic isoprenoid tail of $Q_B$ is situated in channel II, whereas channel I is occupied by the newly observed $Q_C$ molecule. Each channel is formed by amino acid residues, phytyl chains of chlorins and fatty acid chains of lipids, building a flexible and hydrophobic environment which is a prerequisite for PQ/$PQH_2$ diffusion. A closer look on the amino acid residues and cofactors that are involved in channel formation is given in Table 1, and they are visualized in Fig. 8.

The opening of channel I is surrounded by the TMHs of PsbE and PsbF (α- and β-subunit, respectively, of cyt *b559*) and PsbJ, while the opening of channel II is flanked by the TMH of PsbE, PsbF and PsbX (Fig. 8C). Both channels, with dimensions of $10\times20$ Å$^2$ (channel I) and $10\times12$ Å$^2$ (channel II) [226], end directly in the fatty acid environment of the membrane interior. The high lipophilicity of the channels is achieved by the phytyl chains of $Chl_{D2}$, $Chlz_{D2}$ and $Pheo_{D2}$ as well as by $Car_{D2}$ (Car D358) and Car J115 (Table 1 and Fig. 8A). Several lipids (Table 1), namely PG A371, SQDG A372, PG A374 and MGDG E218 at the cytoplasmic side and MGDG D359, DGDG C490, DGDG C491 and MGDG C492 at the lumenal side, form a bilayer structure within PSIIcc close to channel I. Those lipids of the bilayer that are closest to channel I are shown in Fig. 8B to illustrate that their fatty acid chains are involved in building the channel walls. The fatty acid chains of the channel forming lipids are not completely resolved due to their flexibility and the limited resolution of the structural data. The channel walls are also endowed with amino acids side chains, mostly hydrophobic phenylalanine and leucine. Towards the channel exits, polar amino acid residues like serine and threonine are located (Table 1, Fig. 8D). Interestingly, the reoxidation of $PQH_2$ at cyt $b_6f$ takes place in a similar cavity also formed by lipids and thus featuring a suitable region for quinone diffusion [226].

### 6.2. Mechanisms of quinone diffusion

The hydrophobic quinone electron shuttle has to cross the PSIIcc interior and the membrane phase. Three different mechanisms are considered for the exchange of PQ and $PQH_2$ so far [11,15]. They include the two quinone transfer channels I and II, and the $Q_C$ binding site. In the "alternating mechanism" the two channels are alternately used for entry and exit of quinone and quinol molecules. In the "wriggling mechanism" the entry of the quinone proceeds through channel I and the exit of the quinol through channel II exclusively. In the "single channel mechanism" the quinone makes only use of channel II for reduction and protonation, whereas $Q_C$ is not involved in PQ/$PQH_2$ exchange. At present, it cannot be decided, which mechanism applies. A key question in this respect is, whether $Q_C$ is a PQ in a "waiting position" to enter the $Q_B$ site or is involved in other redox reactions (Section 7).

Another important point is that the head group of $PQH_2$ is more polar than that of PQ and is therefore supposed to occupy more polar membrane regions, i.e., closer to the membrane surface [227]. A closer look at the openings of channels I and II reveals that they are not equivalent: The opening of channel I is located in the center of the membrane and that of channel II is slightly closer to the cytoplasmic surface. This can be seen from the positions of amino acid residues of PsbJ and PsbX flanking the channels (Table 1, Fig. 8C, D): Those of PsbJ (channel I) are positioned in the center of the TMH, those of PsbX are closer to the cytoplasmic end of the TMH. If this difference is significant, it would suggest that channel I is designed to take up the more unpolar PQ from the central region of the membrane (PQ inlet channel), whereas channel II is optimized to direct $PQH_2$ towards the more polar membrane region ($PQH_2$ outlet channel). This interpretation would favor the "wriggling mechanism" and assign to $Q_C$ the role of a waiting quinone that has just entered the inlet channel.

### 6.3. Anionic lipids close to the $Q_B$ site

Numerous studies were performed in order to investigate the functional and structural role of lipids that influence photosynthetic ET [228,229]. The neutral lipids MGDG and DGDG are considered to function rather as structural lipids, whereas the anionic PG and SQDG are discussed to be directly involved in the functionality of the acceptor side.

Although the crystal structures of PSIIcc did not reveal PG close to the $Q_B$ site until the 2.9 Å resolution became available [11], biochemical data already pointed to a special role for this lipid [228,230–232]. The manipulation of PG and SQDG led to an impairment of oxygen evolution in most cases ([233] and references therein]. In PSIIcc from *T. vulcanus*, treatment with phospholipase $A_2$, reducing the content of PG, led to a decrease of oxygen evolution by about 40%. In contrast, a diminished content of MGDG due to the addition of lipase caused only an insignificant reduction of oxygen evolution [234]. This finding also indicates that PG plays a crucial role for the function of the ET at the acceptor side compared to the neutral lipids. Possible effects on the donor side are discussed elsewhere [235]. Cells of *Synechocystis* sp. PCC6803, which are defective in phosphatidylglycerolphosphate synthase and therefore incapable of synthesizing PG, show a debilitation of the functionality of $Q_B$ [236]. It was demonstrated that PG deprivation

**Table 1**
Amino acid residues and cofactors flanking the quinone diffusion pathways in PSIIcc. Residues with polar side chains pointing towards the channels are marked in bold-italics. Numbers in parentheses refer to the numbering of residues in Fig. 8D.

| | Channel I | Channel II |
|---|---|---|
| PsbA | Phe A211 (1), Met A214 (2), Leu A218 (3), Ile A259 (4), Ala A263 (5), Phe A265 (6), Leu A271 (7), Phe A274 (8), Trp A278 (9) | Phe A211 (1), Met A214 (2), Leu A218 (3), Ile A259 (4), Ala A263 (5), Phe A265 (6), Leu A271 (7), Phe A274 (8) |
| PsbD | – | Phe D38 (10), Pro D39 (11), ***Tyr D42***, Leu D43 (12) |
| PsbE | Trp E20 (13), ***Ser E24***, Ile E27 (14), Pro E28 (15), Phe E31 (16) | – |
| PsbF | ***Thr F30***, Ile F31 (17), Leu F34 (18) | Val F21 (19), Ala F22 (20), ***Thr F25***, Leu F26 (21), |
| PsbJ | Val J16 (22), Ala J17 (23), Gly J18 (24), Gly J20 (25), Val J21 (26), Val J23 (27) | – |
| PsbX | – | Leu X32 (28), ***Thr X33***, Val X36 (29), |
| Chlorins | $Chl_{D2}$ (phytyl chain) | $Chl_{D2}$ (phytyl chain), $Pheo_{D2}$, $Chlz_{D2}$ |
| Carotenoids | $Car_{D2}$ (Car D358), Car J115 | – |
| Lipids | MDGD E218, SQDG A372, PG A374, DGDG C491, MDGD D359 | MDGD E218, SQDG F224, DGDG D362 |

specifically inactivates $Q_B$ by a suggested structural alteration at the $Q_B$ site and assumed PG to be an intrinsic structural component required for the proper function of the ET. These observations were supported by continuative studies on other cyanobacteria and plants, showing an inhibition of the electron transfer from $Q_A$ to $Q_B$ due to a reduced content of PG [72,234–236]. For the latest review on lipid–PSII interactions, see [71].

In cyanobacterial PSIIcc from *T. elongatus*, the charged phosphate groups of the two PG molecules are located at distances of about 13 and 19 Å from the headgroup of $Q_B$ (with the latter PG being closer to $Q_A$) and 17 Å from each other [11]. They likely have only an indirect influence on the redox properties of the quinones (see also Section 10). By analogy, bRC from *R. sphaeroides* has a negatively charged lipid, but instead of PG, a diphosphatidylglycerol named cardiolipin (CL). This CL is bound at the protein surface about 16 Å away from $Q_B$ [63] and at the opposite side of the RC compared to PG in cyanobacterial PSIIcc. It is probably required to stabilize the protein structure, which might have a positive impact on ET reactions [237].

## 7. Cytochrome *b*559 and side-path electron transfer

The X-ray crystal structure analyses revealed that the heterodimer formed by subunits PsbE (α) and PsbF (β) of cyt *b*559 is located in close proximity to protein D2 (PsbD) of the RC [6–11,16]. Each of these subunits contains a single His residue (E23 and F24 in the sequence numbering of *T. elongatus* [11,62]) and forms one TMH [238–242]. The heme iron is axially ligated by the $N_\varepsilon$ atoms of His E23 and F24 and thus bridges the TMH of these subunits (Fig. 8C). Already earlier spectroscopic analyses indicated that the heme iron is ligated in its fifth and sixth coordination positions by histidine nitrogens. Independently of its valence state (ferric or ferrous), cyt *b*559 was found to be in a low spin state [240,243,244], except for the high potential form (defined below), which was inferred to attain a high spin state based on EPR [245] and Vis absorption data [246].

The heme group of cyt *b*559 is located near the cytosolic surface of PSIIcc [241,247] and is oriented perpendicular to the membrane plane [6–8,10,16]. Based on these X-ray crystal structures, the heme iron of cyt *b*559 is placed at a distance of about 30 Å from the edge of $Q_B$ and 55–60 Å from the metal ions of the WOC [7,8,10,11,16]. The 2.9 Å resolution structure [11] revealed a more detailed insight into the environment of cyt *b*559 compared to previous structures and demonstrated the existence of an additional PQ binding site in agreement with earlier proposals [248,249]. The heme iron of cyt *b*559 is located about ~20 Å apart from the head group of $Q_C$. In addition, structural information is gained from the X-ray data about quinone diffusion pathways (Section 6) revealing that the heme group of cyt *b*559 is located in the vicinity of and between the two channels (Fig. 8A, C).

The light-induced reduction and oxidation of the heme iron is one of the crucial properties of cyt *b*559, which is possibly involved in the regulation of photochemical efficiency of PSII, but does not participate in the primary ET reactions discussed above [250–252]. Depending on the structural integrity and composition of the PSII preparations, at least four different forms of cyt *b*559 can be distinguished on the basis of redox-titrations: the high-potential (HP) form with a redox midpoint potential of $E_m$ ~ 400 mV, the intermediate-potential (IP) form ($E_m$ ~ 200 mV) and the low-potential (LP) form ($E_m$ ~ 50 mV) [246,253–258], and the very low potential (VLP) form ($E_m$ ~ −45 mV) [259].

The origin of the different redox forms of cyt *b*559 and their functional role is not yet clarified. The following possibilities have been discussed for the modulation of the redox properties of the heme group: (i) variation of the mutual orientation of the two planes of the axial histidine ligands of the heme group [240], (ii) modifications of the protonation and/or hydrogen-bonding pattern of axial ligands [253,258,260–262], (iii) changes in the polarity of the dielectric environment of the heme [263], (iv) changes in the nature of heme coordination [246], or (v) binding of PQ to the $Q_C$ site [249]. The transformation of the HP cyt *b*559 into the IP or a mixture of the IP and LP forms are induced by different parameters including temperature and high pH-values, increased salt and detergent concentrations and aging [246,253,254,256,264–270].

Inspite of extensive studies in recent decades, the physiological role of cyt *b559* still remains an enigma [251,252,264]. A number of hypotheses have been put forth to explain the function of cyt *b*559: (i) protection against light stress [251], (ii) plastoquinol oxidase [248,271,272], (iii) superoxide oxidase and reductase [273] and (iv) role in the assembly of PSII [274–277].

(i) A common view considers the participation of cyt *b559* in a cyclic ET pathway, which contributes to the protection of PSII against photoinhibition [278]. At cryogenic temperatures, not only the ET from $Q_A^{\bullet-}$ to $Q_B$ is inhibited (Section 5), but also the reduction of $P_{D1}^{\bullet+}$ by the WOC via $Y_Z$ with half-inhibition temperatures depending on the redox state of the $Mn_4Ca$ cluster [279]. In 40–50% of the centers, $Y_Z$ can still be oxidized by $P_{D1}^{\bullet+}$ [280], giving rise to characteristic metalloradical EPR signals of the coupled $Y_Z^{\bullet}Mn_4Ca$ system [281,282]. In the remaining centers, $P_{D1}^{\bullet+}$ is able to extract electrons (albeit at low rates) from other cofactors in competition to charge recombination with $Q_A^{\bullet-}$, if cyt *b*559 is already in its oxidized state. Spectroscopic studies provide evidence that the oxidized cofactors are Car and/or Chl species, but the identity of these species is under debate [70,252,283,284]. Recent data suggest that the oxidized species is mainly $Car_{D2}$ [83], but a redox equilibrium with other cofactors (e.g., $Chlz_{D2}$), that depends on experimental conditions, cannot be excluded. However, when cyt *b*559 is in its reduced state, it donates an electron to $Car_{D2}^{\bullet+}$ (or $Chlz_{D2}^{\bullet+}$), so that the latter can no longer be detected. These findings show that cyt *b*559 is ultimately able to reduce $P_{D1}^{\bullet+}$ and lend support to a hypothetical protection mechanism, in which a secondary ET process (blue arrows in Fig. 2A) reduces the population probability of this potentially harmful oxidant. Although the heme of cyt *b*559 is localized close to the electron acceptor side of PSIIcc and far away from the WOC (55–60 Å) [6–11], the molecular states of cyt *b*559 are influenced by the integrity of the $Mn_4Ca$ cluster [254]. This "long-range influence" mediated by the protein is reminiscent of the donor side effects on the midpoint potential of $Q_A$ [148] (Section 4.2). The possible physiological role of the cyt *b*559 redox forms [285,286] during the assembly/photoactivation cycle of PSII is discussed in the literature in detail [287,288]. The effect of illumination on the redox properties of cyt *b*559 was studied using PSII membranes from spinach with different integrity of the PSII donor side [289], and the role of cyt *b*559 in the stabilization of oxygen evolution, during photoactivation and/or as a proton acceptor during the WOC turnover has been considered [290–292].
In most samples of PSII membranes deprived of the WOC, the HP form is converted into the IP and LP forms of cyt *b*559, but removal of a functionally competent WOC by gentle treatment does not seriously affect the HP-form [246,257]. Therefore, a strict relation between the functional state of the WOC and the redox properties of cyt *b559* does not exist. Illumination of PSII membranes with an intact WOC gave rise to a small extent of photoreduction of the HP form of cyt *b*559, whereas the IP and the LP forms of cyt *b*559 were unaffected. Moreover, the photoreduction of cyt *b*559 in PSII membranes with an intact WOC was inhibited by herbicides (e.g., DCMU (3-(3,4-dichlorophenyl)-1,1-dimethylurea)), whereas in the membranes lacking the WOC, photoreduction and photooxidation of cyt *b*559 were completely diminished by exogenous superoxidase dismutase (SOD). Interestingly, no effect of SOD on photoreduction of the heme iron was observed in intact PSII membranes. Based on these experiments, Sinha et al. [289] proposed that in PSII membranes with intact WOC the

photoreduction of the heme iron is mediated by plastoquinol, whereas in PSII membranes deprived of WOC, photoreduction and photooxidation are mediated by $O_2^{\bullet-}$ formed by PSII (see below).

(ii) Cyt *b*559 has been proposed to function as a catalyst for the oxidation of the reduced PQ pool by molecular oxygen [248,271,272]. It could be demonstrated that plastoquinones affect the redox state of cyt *b*559 in a way that suggests the presence of a PQ binding site distinct from $Q_B$ and close to cyt *b*559, termed "$Q_C$" [248]. A similar conclusion was drawn from the observation that certain herbicides not only block the $Q_B$ site, but apparently influence the redox potential of cyt *b*559 by binding at a position different from $Q_B$ [249].

(iii) It is known from previous studies that oxygen can be reduced to superoxide by cofactors at the acceptor side prior to $Q_B$ [110,111,273,289,293–295]. Illumination of PSII membranes deprived of the WOC caused photoreduction and photooxidation of IP and HP forms of cyt *b*559, respectively. Since the redox midpoint potential of the IP form of cyt *b559* is in the range of 125–240 mV at pH 7 [249,296–298], the reduction of the IP form of cyt *b*559 by plastoquinol is thermodynamically unfavored. Therefore, it appears to be more likely that another reductant might provide an electron. The finding, that the photooxidation and photoreduction of the heme were completely eliminated by exogenous SOD (see above), suggests that $O_2^{\bullet-}$ serves as reductant and oxidant of cyt *b*559. Indeed, recent studies have demonstrated that $O_2^{\bullet-}$ interacts with the heme iron [273]. It has been suggested that the IP form of cyt *b*559 serves as superoxide oxidase (SOO) which catalyzes the oxidation of $O_2^{\bullet-}$ to $O_2$. Since the midpoint redox potential of the $O_2/O_2^{\bullet-}$ redox couple is −160 mV (pH 7) [299], the reduction of the IP form of cyt *b*559 by $O_2^{\bullet-}$ is thermodynamically possible. Recently, studies of Sinha and coworkers [289] have demonstrated that the HP form of cyt *b*559 acts as superoxide reductase (SOR) known to catalyze the reduction of $O_2^{\bullet-}$ to $H_2O_2$. Assuming that the midpoint redox potential of the $O_2^{\bullet-}/H_2O_2$ redox couple is 890 mV (pH 7) [299], the oxidation of the HP form of cyt *b*559 by $O_2^{\bullet-}$ is thermodynamically favored. Guskov and coworkers have shown in their crystal structure of PSIIcc at 2.9 Å resolution [11] that the putative $PQ/PQH_2$ exchange channel I passes through the $Q_C$ site, while both channels I and II have contact with the $Q_B$ site and are close to cyt *b*559 (Section 6). It was proposed that these channels facilitate diffusion of $O_2^{\bullet-}$ from the acceptor side prior to $Q_B$ (where it is formed [110]) toward the heme and therefore promote oxidation of the iron by $O_2^{\bullet-}$ [289].

(iv) Recent progress in understanding the de novo assembly of PSIIcc suggests a pivotal role for cyt *b*559 [66]. Evidence for a PsbDEF (or D2-cyt *b*559) assembly pre-complex has been reported for barley etioplasts (chloroplasts that have not been exposed to light) [276] and *Synechocystis* sp. PCC 6803 [300]. Studies on PsbE- and PsbEFLJ-deletion mutants indicate that cyt *b*559 is required for PSIIcc assembly in *Chlamydomonas reinhardtii* [274] and for PsbD synthesis and accumulation in *Synechocystis* [301], respectively. Also, cyt *b*559 is able to accumulate in the membrane in the absence of D1 and D2 [301]. The idea emerges from these data that cyt *b*559 acts as a nucleation factor that initiates PSII assembly: First, A D2-cyt *b*559 pre-complex is formed [300,301]. After addition of D1 and PsbI [302] an RC-like pre-complex is constituted [300]. These processes within the thylakoid membrane might be controlled by redox reactions. At a later stage of assembly, a complex is formed, that lacks PsbC (CP43) and the associated LMW as well as the membrane-extrinsic subunits, and is called the RC47 complex [65,66]. RC47 is able to oxidize $Y_Z$, but not water. It is possible that cyt *b*559 acts to protect RC47 against unwanted photochemical reactions initiated by $P_{D1}^{\bullet+}$. However, the assembly of PSII subunits remains enigmatic.

## 8. Role of quinones in photoinhibition

Light is not only the essential energy source of photosynthesis, it is also able to induce destructive processes in all components of the photosynthetic apparatus. Under high light intensities, it is impossible for the metabolic processes to keep up with the electron flow produced by the primary photoreactions and, consequently, the photosynthetic activity decreases. This light-induced physiological stress is generally known as photoinhibition and was discovered more than 100 years ago [303]. It can occur in both photosystems, I and II, but PSII was found to be the major site of photoinhibition [287,304].

### 8.1. Photoinhibition in photosystem II

The D1 subunit of PSII is the main target of photodamage, which occurs actually at all light intensities. Hence, D1 has the highest turnover rate of all PSII subunits [305,306]. Photoinhibition happens only when the repair cycle (for reviews, see [66,304]) of the damaged D1 subunit is not able to cover the caused damage and thus, D1 is degraded faster than it is replaced. It is distinguished between three forms of photoinhibition in PSII: the donor side and the acceptor side induced photodamage and the low light syndrome. Donor side induced inactivation occurs once the $Mn_4Ca$ cluster is not functional, due to the removal of Mn and/or $Ca^{2+}$ ([307,308] and references therein). In acceptor side induced photoinhibition as well as under very low light conditions, highly toxic ROS – such as singlet oxygen ($^1O_2$) – can be formed through charge recombination processes, thereby creating oxidative damage [309–313]. Here, we summarize the current knowledge about acceptor side induced photodamage leading to photoinhibition and focus on the role of the primary electron acceptor $Q_A$.

In the mechanism of acceptor side induced photodamage, PQ from the PQ pool is not sufficiently available, because the subsequent supply with reoxidized PQ – through secondary metabolic processes – is not able to keep pace with the electron flow from PSII. Therefore, the ET from $Q_A^{\bullet-}$ to $Q_B$ or $Q_B^{\bullet-}$ is slowed down or interrupted due to an unoccupied $Q_B$ site. In this situation, charge separated states can be formed such as $S_2Q_A^{\bullet-}$, $S_2Q_B^{\bullet-}$ or $S_3Q_B^{\bullet-}$ ($S_i$ refers to the redox state of the WOC [14,35,36]). These states can give rise to the formation of singlet oxygen, as they can recombine to $P_{D1}^{\bullet+}Q_A^{\bullet-}$. From this state, there are several possible pathways (Fig. 9):

(a) Non-radiative recombination to the ground state via direct tunneling in about 1.7 ms [314].

(b) Indirect non-radiative recombination: $P_{D1}^{\bullet+}Q_A^{\bullet-}$ recombines to $P_{D1}^{\bullet+}Pheo_{D1}^{\bullet-}$. This state has again several options eventually producing $^1O_2$. (i) The singlet state $^1[P_{D1}^{\bullet+}Pheo_{D1}^{\bullet-}]$ undergoes intersystem crossing to the triplet state $^3[P_{D1}^{\bullet+}Pheo_{D1}^{\bullet-}]$, which in turn recombines to an excited triplet state of the RC, $^3$Chl (also referred to as "$^3P_{680}$"). This latter state is likely $^3Chl_{D1}$ in equilibrium with $^3P_{D1}$ [83] and can act as sensitizer to produce $^1O_2$. However, $^3$Chl can also decay non-radiatively into the ground state in ~800 ps in the absence of oxygen [315]. (ii) $^1[P_{D1}^{\bullet+}Pheo_{D1}^{\bullet-}]$ recombines to the ground state (> 1 ns [141,218]). (iii) $^1[P_{D1}^{\bullet+}Pheo_{D1}^{\bullet-}]$ recombines to the singlet excited state $^1P^*$ of the RC ($P^*$ in Section 3.1). $^1P^*$ in turn can transfer excitation energy back to the antenna system [82,141] or decay radiatively (fluorescence) or non-radiatively (internal conversion) to the ground state [141,316]. (iv) $^1[P_{D1}^{\bullet+}Pheo_{D1}^{\bullet-}]$ donates an electron to $Q_A^{\bullet-}$. The doubly reduced quinone may be protonated and leave the RC [310,317]. Then, forward ET is blocked and further excitation of the RC yields the state $P_{D1}^{\bullet+}Pheo_{D1}^{\bullet-}$ that can react as in (i–iii).

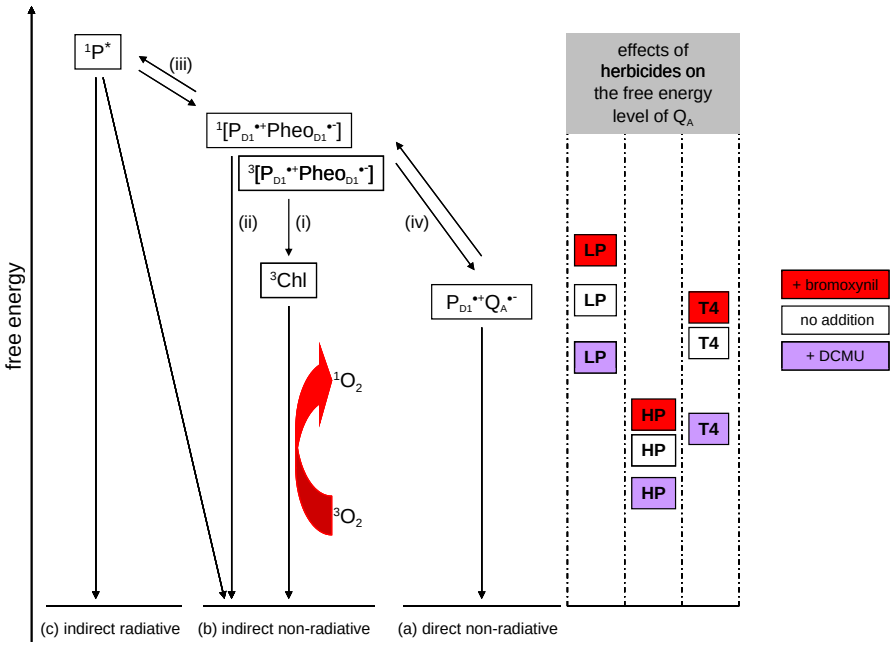


**Fig. 9.** Scheme for possible charge recombination pathways of the $P_{D1}^{\bullet+}Q_A^{\bullet-}$ state and the influence of the free energy level of $Q_A$. Once the states $S_iQ_B^{\bullet-}$ recombined to $P_{D1}^{\bullet+}Q_A^{\bullet-}$, several pathways are possible (for a detailed description of the steps, see text Section 8.1): (a) Non-radiative recombination of $P_{D1}^{\bullet+}Q_A^{\bullet-}$ to the ground state. (b) Indirect non-radiative recombination of $P_{D1}^{\bullet+}Q_A^{\bullet-}$ via the singlet $^1[P_{D1}^{\bullet+}Pheo_{D1}^{\bullet-}]$ or triplet $^3[P_{D1}^{\bullet+}Pheo_{D1}^{\bullet-}]$ state of $P_{D1}^{\bullet+}Pheo_{D1}^{\bullet-}$. The triplet radical pair decays non-radiatively via $^3Chl$ to the ground state, thereby producing likely singlet oxygen $^1O_2$ upon contact with triplet oxygen $^3O_2$ (red arrow). The singlet radical pair can also decay non-radiatively via direct recombination or recombine to $^1P^*$, which decays non-radiatively. (c) Indirect radiative recombination of $P_{D1}^{\bullet+}Q_A^{\bullet-}$ via $^1[P_{D1}^{\bullet+}Pheo_{D1}^{\bullet-}]$ to $^1P^*$, which decays to the ground state by light emission. The free energy level of $Q_A$ is different in the LP or HP form of spinach and in the T4 mutant from *B. viridis* (white boxes). The addition of the phenolic herbicide bromoxynil (red boxes) shifts the free energy levels of $Q_A$ towards lower values, thereby decreasing the energy gap between $P_{D1}^{\bullet+}Q_A^{\bullet-}$ and $P_{D1}^{\bullet+}Pheo_{D1}^{\bullet-}$, and favoring charge recombination via the $^1O_2$ forming way (red arrow). The addition of the urea herbicide DCMU (purple boxes) has the opposite effect and increases the energy gap between $P_{D1}^{\bullet+}Q_A^{\bullet-}$ and $P_{D1}^{\bullet+}Pheo_{D1}^{\bullet-}$, favoring the harmless charge recombination route (a).

(c) Indirect radiative recombination: $P_{D1}^{\bullet+}Q_A^{\bullet-}$ recombines via $^1[P_{D1}^{\bullet+}\ Pheo_{D1}^{\bullet-}]$ to $^1P^*$, which decays to the ground state by light emission (≈3 ns, [316] and references therein) or transfers the excitation energy to antenna Chl that emit light.

Singlet oxygen is very harmful for its protein environment as it rapidly reacts with carbon–carbon double bonds and also carbon–sulfur bonds, thereby damaging amino acids, lipids and pigments. The formation of singlet oxygen through a triplet forming charge recombination way is considered to be one of the main sources for destruction of the PSII reaction center, drastically decreasing its photosynthetic activity [287,304,318,319]. Therefore, it is of high interest to identify the parameters that influence the charge recombination pathway and determine the yield of the different routes of electron back flow. In the following the influence of the midpoint redox potential of the primary quinone $Q_A$ will be depicted.

### 8.2. Influences of the $Q_A$ redox potential on charge recombination pathways

First knowledge about the influence of the $Q_A$ redox potential on the yield of the different charge recombination pathways was obtained from studies with bRC. It was observed, that the used route for charge recombination is determined by the free energy gap between $H_A$ and $Q_A$ [131,320]. Thus, in PSII the pathway of charge recombination was expected to be influenced by the free energy level of the involved redox components ($P_{D1}$, $Pheo_{D1}$, and $Q_A$) in a way similar to bRC. The redox midpoint potential ($E_m$) of $Q_A$ in PSII membranes (from spinach) was found to be −80 mV [147,321] and −110 mV in PSIIcc of *T. elongatus* [322], both active in oxygen evolution. The $E_m$ values can vary strongly as a consequence of (i) changes at the donor side, (ii) herbicide binding to the acceptor side or (iii) mutations at the $Q_A$ binding site.

#### 8.2.1. Low and high potential form of $Q_A$

So called "low and high potential" (LP and HP) forms of $Q_A$ were defined by Krieger et al. [147] and were ascribed to the active and inactive (due to $Ca^{2+}$ depletion) stage of oxygen evolution of spinach PSII membranes, respectively. Under a wide variety of conditions, concerning temperature, pH, presence of mediators and oxygen evolving activity, the $Q_A^{\bullet-}$ formation during redox titrations was detected either by Chl *a* fluorescence or EPR signals and essentially confirmed observations already reported in [323]. In a pH range of stable oxygen evolution activity (pH 5.5−7.5), the $E_m$ value of $Q_A$ in active PSII membranes was determined to be about −80 mV (LP), whereas the $E_m$ value shifted to about +65 mV (HP) in inactive samples [147]. Therefore, it was assumed that changes at the donor side (depletion of $Ca^{2+}$ or loss of $Mn_4Ca$ cluster) of the RC cause the $Q_A$ redox potential shift of 150 mV. In studies similar to [147], a low and high potential form of $Q_A$ were also found in PSIIcc of *T. elongatus* and were determined to be −110 mV and +60 mV, respectively [322]. The possible physiological role of the HP and LP form is discussed below.

#### 8.2.2. Effects of herbicides

It has been known for many years, that changes at the $Q_B$ site – such as inhibitor binding – influence the properties of $Q_A$ [122,324]. PSII inhibitors bind with high affinity to the $Q_B$ site, competing with the native quinone molecules, and block the ET from $Q_A$ to $Q_B$ [325]. It was shown, that certain types of herbicides are able to shift the redox potential of $Q_A$ and hence its free energy level [321]. Herbicides are commercially used PSII inhibitors (for review, see [326]) and were divided into two groups, according to their orientation in the binding pocket [327]: classical urea- and triazine-types orienting themselves towards Ser A264 and phenolic derivatives orienting themselves towards His A215. Possible explanations for the interaction of herbicides with specific amino acid residues in the $Q_B$ pocket that lead to the

potential shift and the transmission of the changes to the $Q_A$ site, were provided through FTIR spectroscopy along with density functional theory calculations [328,329]. The results of these studies indicate that in the case of a bound phenolic herbicide, a change in the hydrogen bond strength of the NH group of His A215 influences the strength of the hydrogen bond between His D214 and the C4═O carbonyl group of $Q_A^{\bullet-}$ mediated by the NHI [328,329].

Depending on the type of bound herbicide (classical or phenolic), the photosensivity of PSII was found to be affected in opposite ways. Several in vitro and in vivo studies with plants, algae and cyanobacteria showed a stabilizing effect of urea/triazine-type herbicides on PSII and a decreased photoinhibition, whereas phenolic herbicides destabilize PSII, leading to an increased sensitivity to light [330–334]. A thermodynamic mechanism to explain the origin of these opposed effects was proposed by Krieger-Liszkay and Rutherford [321], based on the found shifts of $E_m(Q_A/Q_A^{\bullet-})$ and thermoluminescence (TL) bands reflecting the stability of the involved charge pairs (for review on TL, see [335]). The redox midpoint potential of $Q_A$ in the presence of the herbicides DCMU, a classical type, or bromoxynil (3,5-dibromo-4-hydroxybenzonitrile), a phenolic type, was determined via titration of Chl *a* fluorescence of spinach membrane fragments. The same effect was observed for both, the LP as well as for the HP form: DCMU increases and bromoxynil decreases the $E_m(Q_A/Q_A^{\bullet-})$ (see Table 2). In accordance with TL measurements, a model for charge recombination (Fig. 9) depending on the free energy gap between $P_{D1}^{+}Q_A^{\bullet-}$ and $P_{D1}^{\bullet+}Pheo_{D1}^{\bullet-}$ was proposed [321]. As DCMU increases this energy gap, the harmless direct recombination pathway (a) (see above and Fig. 9) is more likely. On the other hand, phenolic herbicides decrease the energy difference to $P_{D1}^{\bullet+}Pheo_{D1}^{\bullet-}$ leading to a higher possibility of charge recombination via $^3$Chl formation (b(i)) (Fig. 9) and therefore $^1O_2$ production. These findings are considered to explain the higher rate of photoinhibition of PSII samples in the presence of phenolic herbicides [321].

In vivo fluorescence and TL studies of PSII photoinhibition in the cyanobacterium *Synechococcus* sp. PCC 7942, treated with either DCMU or BNT (2-bromo-3-methyl-6-isopropyl-4-nitrophenol), supported the recombination mechanism proposed by Krieger-Liszkay and Rutherford [321]. A fast photoinhibition and the formation of ROS was only detectable in the presence of BNT [336].

In order to circumvent the fact, that urea-type and phenolic herbicides do not bind to the bRC, a T4 mutant of *B. viridis*, which is sensitive to these herbicides [184], was used to investigate their influence on recombination kinetics and the $Q_A$ redox potential at pH 6.5 [337]. The observed shifts of the $E_m(Q_A/Q_A^{\bullet-})$ are very similar to those in PSII-RC (see Table 2).

### 8.3. Effects of mutations at the $Q_A$ site

Through a single point mutation in the binding pocket of $Q_A$ in *T. elongatus* it was possible to influence the midpoint potential of $Q_A$ and investigate its impact on charge recombination pathways and photoinhibition, independently of the presence of herbicides [338]. Therefore, possible side effects on the process of photodamage and photoinhibition, due to the use of herbicides, could be avoided in this study. In the A(D249)S mutant, Ala D249 which is a residue in the $Q_A$ binding pocket was changed to serine. Compared to the wild type [338], $E_m(Q_A/Q_A^{\bullet-})$ decreased by 60 mV due to the A(D249)S mutation, similar to the situation observed in PSII samples treated with a phenolic herbicide. The influence of the mutation on photoinhibition was detected by monitoring the changes of the Chl fluorescence yield and the oxygen evolving activity in both, in vitro and in vivo experiments. After illumination, the amount of produced oxygen as well as the yield of fluorescence decreased faster in all samples of the A(D249)S mutant compared to the wild type. The addition of herbicides amplified (in the case of bromoxynil) or diminished (in the case of DCMU) this effect. Besides the increased sensibility to light, a higher amount of singlet oxygen was also detected in the mutant as shown in spin-trapping assays using PSII particles. Moreover, TL measurements revealed a $S_2Q_A^{\bullet-}$ charge recombination at lower temperatures in the mutant than in the wild type, indicating a smaller energy gap between $S_2Q_A^{\bullet-}$ and $P_{D1}^{\bullet+}Pheo_{D1}^{\bullet-}$ since less energy is required for the back reaction. The recombination kinetics of the $S_2Q_A^{\bullet-}$ state were also studied via the decay of the fluorescence yield and were found to be faster in the mutant than in the wild type, showing a biphasic behavior [338]. All these observations support the role of the $Q_A$ redox potential in directing the way of charge recombination (Fig. 9) and therefore photoinhibition as it was proposed in the model by Krieger-Liszkay and Rutherford [321].

The free energy gap between $S_2Q_A^{\bullet-}$ and $P_{D1}^{\bullet+}Pheo_{D1}^{\bullet-}$ can also be modified by changing the midpoint potential of the redox components $Pheo_{D1}$ or $P_{D1}$ through site-directed mutagenesis as it was shown in [140,316,339,340]. These changes also influence the kinetics and routes of charge recombination.

### 8.4. Protection against photoinhibition by $Q_A$ potential changes

The possibility of modulating the redox potential of $Q_A$ and also $Pheo_{D1}$ provides a way for photosynthetic organisms to protect themselves against oxidative stress. With changes in these redox potentials, the formation of the potentially harmful radical pair states (b(i)) can be avoided as the harmless non-radiative charge recombination (a) becomes the dominant pathway (see Fig. 9).

Cyanobacteria possess different gene copies for the D1 subunit, which are expressed in various yields depending on light conditions [341–343]. The low- and high-light forms of D1 differ in several amino acid positions, but they all feature the replacement of Glu A130 with Gln under high light intensities. This replacement was shown to increase the redox potential of $Pheo_{D1}$, leading to an accelerated charge recombination and a reduced light sensitivity. The latter two effects were proposed to originate from the decreased recombination via the triplet forming routes (b(i)) [316,344–346].

By inactivating PSII through the depletion of $Ca^{2+}$ or loss of the $Mn_4Ca$ cluster, the potential of $Q_A$ is shifted from the LP to the HP form. This effect presents a direct influence of the donor side situation on the properties of the acceptor side. This mechanism is supposed to play an important role in protecting PSII against photodamage during the assembly of the RC, also by increasing the efficiency of pathway (a) (Fig. 9) [147,148,347]. The role of $E_m(Q_A/Q_A^{\bullet-})$ in active PSII samples in controlling the charge recombination routes was strongly supported by the A(D249)S mutant investigated in [338] independently of the addition of herbicides. Still, it remains interesting to study how herbicides, which bind at the $Q_B$ site, are able to influence the redox potential of $Q_A$. First prospects were gained through spectroscopic and theoretical investigations [328,329] and could be supported recently through the attainment of the first crystal structure of a PSIIcc/terbutryn complex [348].

**Table 2**
Redox midpoint potential of $Q_A$ (in mV) with and without the addition of herbicides. Values are taken from [321] for spinach membranes and [337] for the *B. viridis* T4 mutant.

| | No addition | + DCMU | + bromoxynil |
|---|---|---|---|
| PSII: LP form | −80 ± 16 | −28 ± 18 | −125 ± 16 |
| PSII: HP form | +73 ± 17 | +123 ± 5 | +24 ± 14 |
| bRC: *B. viridis* T4 mutant | −57 ± 10 | +55 ± 25 | −77 ± 35 |

## 9. Conclusion and perspectives

The quinone reductase part of PSIIcc is often outshined by the huge interest in the water oxidase part, but it is neither less interesting nor less complicated. Also, there is a connection between the two parts that actually prohibits to consider them separately. On the other hand, space limitations do not allow to treat both aspects with the same rigor in one

review. Here, we have made an attempt to collect experimental and theoretical data, concerning quinones in PSIIcc, as a basis for an understanding of the crystal structures and to establish a connection to topics of physiological interest such as regulation of ET and photoinhibition/photoprotection. Much has been learned about the acceptor side of type-II RC from studies on bRC, but the comparability to PSII-RC is limited, since the two systems are adapted to a different metabolic context. This is particularly evident from the binding of (bi)carbonate to the NHI. We consider the clarification of the role of (bi)carbonate in this position as one of the key topics of future research as it likely regulates both ET and PT to $Q_B$. In this respect, the identification of protein-bound water molecules will be important. Although not possible at 2.9 Å resolution, the crystal structure at 1.9 Å resolution [16] provides this information (Section 10). Other topics of prime interest are the role of lipids within PSIIcc, the relationship between quinone diffusion pathways and the still elusive function of cyt *b*559, as well as the connection between herbicide binding to the $Q_B$ site and the relevance of $Q_A$ redox potential shifts for photoinhibition. From the viewpoint of structural biology, progress has been made in these areas by the identification of new lipid cofactors [10,11,226], the discovery of a novel quinone binding site $Q_C$ [11] and the first elucidation of a PSIIcc crystal structure with a herbicide bound to the $Q_B$ pocket [348]. Future work along these lines will focus on the questions how the loss of lipids during the preparation and purification steps of PSIIcc can be minimized, how the presence and position of $Q_B$/$Q_C$ depend on experimental conditions (by analogy to the various $Q_B$ positions in bRC) and how different types of herbicides bind to the $Q_B$ site. Finally, the conformational connection between donor and acceptor side needs further investigation. PSIIcc has two faces, and both are worth a closer look.

## 10. Addendum: the 1.9 Å resolution crystal structure

After completion of the manuscript, Umena at al. [16] published the crystal structure of dimeric PSIIcc from *T. vulcanus* at 1.9 Å resolution (PDB entry 3ARC). Clearly, the most intriguing aspect is that a reliable structure of the WOC was obtained, which turns out to be a $Mn_4CaO_5$ cluster (for more details as regards the WOC, see the very recent review by Kawakami et al. [349]). Here, we summarize information from the new crystal structure concerning the topics of this review.

Not surprisingly, the cofactor inventory observed in the structure at 1.9 Å resolution in *T. vulcanus* is mostly the same as that at 2.9 Å resolution in *T. elongatus*, but there are some slight differences: the β-carotene $Car_{15}$ identified in *T. elongatus* is not found at the higher resolution in *T. vulcanus*. In the latter structure, there are only 6 MGDG, 5 DGDG, and 4 SQDG per monomer compared to 11, 7, and 5 lipid molecules, respectively, in the less resolved structure. In contrast, the PG content in the structure at 1.9 Å resolution is higher with 5 molecules per monomer compared to 2 at 2.9 Å resolution. Both structures contain detergent molecules. There are 5 molecules of βDM per monomer present in the crystal structure at 1.9 Å resolution compared to 7 at 2.9 Å resolution. In addition, the 1.9 Å resolution structure features 8–9 molecules of n-heptyl-β-D-thioglucoside (HTG) per monomer. This comes somewhat as a surprise, as the use of HTG is neither reported in reference [16] nor in the cited methods [350,351]. At this point it has to be mentioned, that the use of a different detergent influences the crystallization behavior and the intramolecular protein and detergent contacts in the crystal [352]. Therefore, this issue should also be discussed regarding the highly improved resolution of the crystal structure. Variations of detergent concentration and composition used in the different laboratories are most likely a reason for the disparities in the carotenoid, lipid and detergent content of PSIIcc. Indeed, two of the βDM molecules found in the cytoplasmic lipid/detergent-layer at the monomer–monomer interface assigned in the 1.9 Å resolution structure seem to replace MDGD found at 2.9 Å resolution. Replacements of this kind are expected due to the similarity of the sugar headgroups (see Section 2.2.). On the other hand, the three new PG molecules per monomer found in the structure at 1.9 Å resolution are located at sites occupied by MDGD at 2.9 Å resolution. Possible reasons for this finding could be (i) a misassignment of lipids in the lower resolution structure or, more likely, (ii) differences in the lipid composition of PSIIcc that could be species-specific and/or dependent on growth conditions. The latter aspect is of particular interest, as the phosphate group of one of the new PG molecules is located at a close distance of about 8 Å from $Q_A$ [16] and thus could influence ET reactions to a greater extent than any of the PG molecules at the $Q_B$ side. These problems require further research.

The LMW subunit PsbY, which is located close to cyt *b*559 [11,353], is not found in the 1.9 Å resolution structure [16], because it has presumably been lost during purification/crystallization as reported in other crystallographic studies [8,12]. In the 2.9 Å resolution crystal structure, it could only be modeled as poly-Ala due to a poor electron density in this region [11,15]. So, it remains a challenge for crystallography to unravel structural details of this subunit and its interaction with cyt *b*559. Likewise, $Q_C$ is not detected in the 1.9 Å resolution structure. Again, this result does not necessarily indicate a misassignment in the earlier structure, but can rather be taken as a sign of an ill-defined and preparation-dependent position that would be expected, if $Q_C$ was indeed a substrate quinone.

Another important aspect of the 1.9 Å resolution structure is the localization of more than 1300 water molecules per PSIIcc-monomer [16]. Interestingly, the $Q_B$ site is essentially devoid of water molecules, but there is one interacting with His A252, and two water molecules bridge Glu A244 and Tyr A246. These waters appear to mark two proton transfer pathways to each of the two carbonyl groups of the quinone. By analogy with the bRC (cf. Section 5.2), it is tempting to presume that the first proton enters via His A252 and Ser A264 (instead of Asp L213 and Ser L223 in bRC), while the second proton arrives via Tyr A246 (instead of Glu L212, cf. Fig. 6). The route via Tyr A246 likely involves Glu A244 and is influenced by the presence of the (bi)carbonate anion (Fig. 4A).

## Acknowledgements

We thank Dr. A. Gabdulkhakov and Dr. A. Guskov for providing material to generate Figs. 7 and 8 as well as Prof. G. Renger for critical comments on the manuscript. This work was supported by the DFG-Cluster of Excellence "UniCat" coordinated by the Technische Universität Berlin.

## References

[1] P. Jordan, P. Fromme, H.T. Witt, O. Klukas, W. Saenger, N. Krauss, Three-dimensional structure of cyanobacterial photosystem I at 2.5 Å resolution, Nature 411 (2001) 909–917.
[2] A. Ben-Shem, F. Frolow, N. Nelson, Crystal structure of plant photosystem I, Nature 426 (2003) 630–635.
[3] A. Amunts, H. Toporik, A. Borovikova, N. Nelson, Structure determination and improved model of plant photosystem I, J. Biol. Chem. 285 (2010) 3478–3486.
[4] G. Kurisu, H. Zhang, J.L. Smith, W.A. Cramer, Structure of the cytochrome $b_6f$ complex of oxygenic photosynthesis: tuning the cavity, Science 302 (2003) 1009–1014.
[5] D. Stroebel, Y. Choquet, J.L. Popot, D. Picot, An atypical haem in the cytochrome $b_6f$ complex, Nature 426 (2003) 413–418.
[6] A. Zouni, H.T. Witt, J. Kern, P. Fromme, N. Krauss, W. Saenger, P. Orth, Crystal structure of photosystem II from *Synechococcus elongatus* at 3.8 Å resolution, Nature 409 (2001) 739–743.
[7] N. Kamiya, J.R. Shen, Crystal structure of oxygen-evolving photosystem II from *Thermosynechococcus vulcanus* at 3.7 Å resolution, Proc. Natl. Acad. Sci. U.S.A. 100 (2003) 98–103.
[8] K.N. Ferreira, T.M. Iverson, K. Maghlaoui, J. Barber, S. Iwata, Architecture of the photosynthetic oxygen-evolving center, Science 303 (2004) 1831–1838.
[9] J. Biesiadka, B. Loll, J. Kern, K.D. Irrgang, A. Zouni, Crystal structure of cyanobacterial photosystem II at 3.2 Å resolution: a closer look at the Mn-cluster, Phys. Chem. Chem. Phys. 6 (2004) 4733–4736.
[10] B. Loll, J. Kern, W. Saenger, A. Zouni, J. Biesiadka, Towards complete cofactor arrangement in the 3.0 Å resolution structure of photosystem II, Nature 438 (2005) 1040–1044.

[11] A. Guskov, J. Kern, A. Gabdulkhakov, M. Broser, A. Zouni, W. Saenger, Cyanobacterial photosystem II at 2.9 Å resolution: role of quinones, lipids, channels and chloride, Nat. Struct. Mol. Biol. 16 (2009) 334–342.
[12] M. Broser, A. Gabdulkhakov, J. Kern, A. Guskov, F. Müh, W. Saenger, A. Zouni, Crystal structure of monomeric photosystem II from *Thermosynechococcus elongatus* at 3.6 Å resolution, J. Biol. Chem. 285 (2010) 26255–26262.
[13] T. Wydrzynski, K. Satoh, Photosystem II: the light-driven water:plastoquinone oxidoreductase, in: Govindjee (Ed.), Advances in Photosynthesis and Respiration, Springer, Dordrecht, 2005.
[14] G. Renger, T. Renger, Photosystem II: the machinery of photosynthetic water splitting, Photosynth. Res. 98 (2008) 53–80.
[15] A. Guskov, A. Gabdulkhakov, M. Broser, C. Glöckner, J. Hellmich, J. Kern, J. Frank, F. Müh, W. Saenger, A. Zouni, Recent progress in the crystallographic studies of photosystem II, ChemPhysChem 11 (2010) 1160–1171.
[16] Y. Umena, K. Kawakami, J.R. Shen, N. Kamiya, Crystal structure of oxygen-evolving photosystem II at a resolution of 1.9 Å, Nature 473 (2011) 55–60.
[17] H. Michel, Three-dimensional crystals of a membrane protein complex. The photosynthetic reaction center from *Rhodopseudomonas viridis*, J. Mol. Biol. 158 (1982) 567–572.
[18] J. Deisenhofer, O. Epp, K. Miki, R. Huber, H. Michel, X-ray structure analysis of a membrane protein complex. Electron density map at 3 Å resolution and a model of the chromophores of the photosynthetic reaction center from *Rhodopseudomonas viridis*, J. Mol. Biol. 180 (1984) 385–398.
[19] J. Deisenhofer, O. Epp, K. Miki, R. Huber, H. Michel, Structure of the protein subunits in the photosynthetic reaction center of *Rhodopseudomonas viridis* at 3 Å resolution, Nature 318 (1985) 618–624.
[20] H. Michel, O. Epp, J. Deisenhofer, Pigment protein interactions in the photosynthetic reaction center from *Rhodopseudomonas viridis*, EMBO J. 5 (1986) 2445–2451.
[21] H. Michel, J. Deisenhofer, Relevance of the photosynthetic reaction center from purple bacteria to the structure of photosystem II, Biochemistry 27 (1988) 1–7.
[22] J. Deisenhofer, H. Michel, The photosynthetic reaction center from the purple bacterium *Rhodopseudomonas viridis*, Science 245 (1989) 1463–1473.
[23] J.P. Allen, G. Feher, Crystallization of reaction center from *Rhodopseudomonas sphaeroides*: preliminary characterization, Proc. Natl. Acad. Sci. U.S.A. 81 (1984) 4795–4799.
[24] J.P. Allen, G. Feher, T.O. Yeates, D.C. Rees, J. Deisenhofer, H. Michel, R. Huber, Structural homology of reaction centers from *Rhodopseudomonas sphaeroides* and *Rhodopseudomonas viridis* as determined by X-ray diffraction, Proc. Natl. Acad. Sci. U.S.A. 83 (1986) 8589–8593.
[25] J.P. Allen, G. Feher, T.O. Yeates, H. Komiya, D.C. Rees, Structure of the reaction center from *Rhodobacter sphaeroides* R-26: the cofactors, Proc. Natl. Acad. Sci. U.S.A. 84 (1987) 5730–5734.
[26] J.P. Allen, G. Feher, T.O. Yeates, H. Komiya, D.C. Rees, Structure of the reaction center from *Rhodobacter sphaeroides* R-26: the protein subunits, Proc. Natl. Acad. Sci. U.S.A. 84 (1987) 6162–6166.
[27] T.O. Yeates, H. Komiya, D.C. Rees, J.P. Allen, G. Feher, Structure of the reaction center from *Rhodobacter sphaeroides* R-26: membrane–protein interactions, Proc. Natl. Acad. Sci. U.S.A. 84 (1987) 6438–6442.
[28] T.O. Yeates, H. Komiya, A. Chirino, D.C. Rees, J.P. Allen, G. Feher, Structure of the reaction center from *Rhodobacter sphaeroides* R-26 and 2.4.1: protein-cofactor (bacteriochlorophyll, bacteriopheophytin, and carotenoid) interactions, Proc. Natl. Acad. Sci. U.S.A. 85 (1988) 7993–7997.
[29] J.P. Allen, G. Feher, T.O. Yeates, H. Komiya, D.C. Rees, Structure of the reaction center from *Rhodobacter sphaeroides* R-26: protein–cofactor (quinones and $Fe^{2+}$) interactions, Proc. Natl. Acad. Sci. U.S.A. 85 (1988) 8487–8491.
[30] H. Komiya, T.O. Yeates, D.C. Rees, J.P. Allen, G. Feher, Structure of the reaction center from *Rhodobacter sphaeroides* R-26 and 2.4.1: symmetry relations and sequence comparisons between different species, Proc. Natl. Acad. Sci. U.S.A. 85 (1988) 9012–9016.
[31] G. Feher, J.P. Allen, M.Y. Okamura, D.C. Rees, Structure and function of bacterial photosynthetic reaction centers, Nature 339 (1989) 111–116.
[32] J. Kern, J. Biesiadka, B. Loll, W. Saenger, A. Zouni, Structure of the $Mn_4$–Ca cluster as derived from X-ray diffraction, Photosynth. Res. 92 (2007) 389–405.
[33] J. Barber, J.W. Murray, Revealing the structure of the Mn-cluster of photosystem II by X-ray crystallography, Coord. Chem. Rev. 252 (2008) 233–243.
[34] H. Dau, M. Haumann, The manganese complex of photosystem II in its reaction cycle—basic framework and possible realization at the atomic level, Coord. Chem. Rev. 252 (2008) 273–295.
[35] J. Messinger, G. Renger, Photosynthetic water splitting, in: G. Renger (Ed.), Primary Processes of Photosynthesis, Principles and Apparatus, RSC Publishing, Cambridge, 2008, pp. 291–349.
[36] F. Müh, A. Zouni, Light-induced water oxidation in photosystem II, Front. Biosci. 16 (2011) 3072–3132.
[37] A.A. Benson, M. Calvin, Carbon dioxide fixation by green plants, Annu. Rev. Plant Physiol. 1 (1950) 25–42.
[38] M. Calvin, 40 years of photosynthesis and related activities, Photosynth. Res. 21 (1989) 3–16.
[39] A.A. Benson, Following the path of carbon in photosynthesis: a personal story, Photosynth. Res. 73 (2002) 31–49.
[40] B. Rumberg, P. Schmidt-Mende, H.T. Witt, Different demonstrations of coupling of 2 light reactions in photosynthesis, Nature 201 (1964) 466–468.
[41] W.A. Cramer, H. Zhang, J. Yan, G. Kurisu, E. Yamashita, N. Dashdorj, H. Kim, S. Savikhin, Structure–function of the cytochrome $b_6f$ complex: a design that has worked for three billion years, in: G. Renger (Ed.), Primary Processes of Photosynthesis, Principles and Apparatus, RSC Publishing, Cambridge, 2008, pp. 417–446.
[42] W.A. Cramer, H. Zhang, J. Yan, G. Kurisu, J.L. Smith, Transmembrane traffic in the cytochrome $b_6f$ complex, Annu. Rev. Biochem. 75 (2006) 769–790.
[43] T. Inoue, H. Sugawara, S. Hamanaka, H. Tsukui, E. Suzuki, T. Kohzuma, Y. Kai, Crystal structure determinations of oxidized and reduced plastocyanin from the cyanobacterium *Synechococcus* sp. PCC 7942, Biochemistry 38 (1999) 6063–6069.
[44] M.R. Sawaya, D.W. Krogmann, A. Serag, K.K. Ho, T.O. Yeates, C.A. Kerfeld, Structures of cytochrome c-549 and cytochrome $c_6$ from the cyanobacterium *Arthrospira maxima*, Biochemistry 40 (2001) 9215–9225.
[45] J.H. Golbeck, Photosystem I — the light-driven plastocyanin:ferredoxin oxidoreductase, in: Govindjee (Ed.), Advances in Photosynthesis and Respiration, Springer, Dordrecht, 2006.
[46] R. Fromme, I. Grotjohann, P. Fromme, Structure and function of photosystem I, in: G. Renger (Ed.), Primary Processes of Photosynthesis, Principles and Apparatus, RSC Publishing, Cambridge, 2008, pp. 111–146.
[47] H. Hatanaka, R. Tanimura, S. Katoh, F. Inagaki, Solution structure of ferredoxin from the thermophilic cyanobacterium *Synechococcus elongatus* and its thermostability, J. Mol. Biol. 268 (1997) 922–933.
[48] P. Sétif, Electron transfer from the bound iron–sulfur clusters to ferredoxin/flavodoxin: kinetic and structural properties of ferredoxin/flavodoxin reduction by photosystem I, in: J.H. Golbeck (Ed.), Photosystem I, The Light-Driven Plastocyanin: Ferredoxin Oxidoreductase, Springer, Dordrecht, 2006, pp. 439–454.
[49] L. Serre, F.M.D. Vellieux, M. Medina, C. GomezMoreno, J.C. FontecillaCamps, M. Frey, X-ray structure of the ferredoxin:$NADP^+$ reductase from the cyanobacterium *Anabaena* PCC 7119 at 1.8 Å resolution, and crystallographic studies of $NADP^+$ binding at 2.25 Å resolution, J. Mol. Biol. 263 (1996) 20–39.
[50] R. Morales, G. Kachalova, F. Vellieux, M.H. Charon, M. Frey, Crystallographic studies of the interaction between the ferredoxin-$NADP^+$ reductase and ferredoxin from the cyanobacterium *Anabaena*: looking for the elusive ferredoxin molecule, Acta Crystallogr. D 56 (2000) 1408–1412.
[51] J.K. Hurley, G. Tollin, M. Medina, C. Gómez-Moreno, Electron transfer from ferredoxin and flavodoxin to ferredoxin:$NADP^+$ reductase, in: J.H. Golbeck (Ed.), Photosystem I, The Light-Driven Plastocyanin:Ferredoxin Oxidoreductase, Springer, Dordrecht, 2006, pp. 455–476.
[52] D.M. Rees, A.G.W. Leslie, J.E. Walker, The structure of the membrane extrinsic region of bovine ATP synthase, Proc. Natl. Acad. Sci. U.S.A. 106 (2009) 21597–21601.
[53] D. Pogoryelov, O. Yildiz, J.D. Faraldo-Gomez, T. Meier, High-resolution structure of the rotor ring of a proton-dependent ATP synthase, Nat. Struct. Mol. Biol. 16 (2009) 1068–1073.
[54] D. Stock, A.G. Leslie, J.E. Walker, Molecular architecture of the rotary motor in ATP synthase, Science 286 (1999) 1700–1705.
[55] W. Junge, Photophosphorylation, in: G. Renger (Ed.), Primary Processes of Photosynthesis, Principles and Apparatus, RSC Publishing, Cambridge, 2008, pp. 447–487.
[56] W. Junge, H. Sielaff, S. Engelbrecht, Torque generation and elastic power transmission in the rotary F(O)F(1)-ATPase, Nature 459 (2009) 364–370.
[57] J. Kern, B. Loll, C. Lüneberg, D. DiFiore, J. Biesiadka, K.D. Irrgang, A. Zouni, Purification, characterisation and crystallisation of photosystem II from *Thermosynechococcus elongatus* cultivated in a new type of photobioreactor, Biochim. Biophys. Acta 1706 (2005) 147–157.
[58] A. Zouni, From cell growth to the 3.0 Å resolution crystal structure of cyanobacterial photosystem II, in: G. Renger (Ed.), Primary Processes of Photosynthesis, Principles and Apparatus, RSC Publishing, Cambridge, 2008, pp. 193–236.
[59] A. Zouni, R. Jordan, E. Schlodder, P. Fromme, H.T. Witt, First photosystem II crystals capable of water oxidation, Biochim. Biophys. Acta 1457 (2000) 103–105.
[60] H. Adachi, Y. Umena, I. Enami, T. Henmi, N. Kamiya, J.R. Shen, Towards structural elucidation of eukaryotic photosystem II: purification, crystallization and preliminary X-ray diffraction analysis of photosystem II from a red alga, Biochim. Biophys. Acta 1787 (2009) 121–128.
[61] D. Piano, S. El Alaoui, H.J. Korza, R. Filipek, I. Sabala, P. Haniewicz, C. Buechel, D. De Sanctis, M. Bochtler, Crystallization of the Photosystem II core complex and its chlorophyll binding subunit CP43 from transplastomic plants of *Nicotiana tabacum*, Photosynth. Res. 106 (2010) 221–226.
[62] F. Müh, T. Renger, A. Zouni, Crystal structure of cyanobacterial photosystem II at 3.0 Å resolution: a closer look at the antenna system and the small membrane-intrinsic subunits, Plant Physiol. Biochem. 46 (2008) 238–264.
[63] J. Koepke, E.M. Krammer, A.R. Klingen, P. Sebban, G.M. Ullmann, G. Fritzsch, pH modulates the quinone position in the photosynthetic reaction center from *Rhodobacter sphaeroides* in the neutral and charge separated states, J. Mol. Biol. 371 (2007) 396–409.
[64] T.M. Bricker, L.K. Frankel, The structure and function of CP47 and CP43 in photosystem II, Photosynth. Res. 72 (2002) 131–146.
[65] A. Rokka, M. Suorsa, A. Saleem, N. Battchikova, E.M. Aro, Synthesis and assembly of thylakoid protein complexes: multiple assembly steps of photosystem II, Biochem. J. 388 (2005) 159–168.
[66] P.J. Nixon, F. Michoux, J.F. Yu, M. Boehm, J. Komenda, Recent advances in understanding the assembly and repair of photosystem II, Ann. Bot. 106 (2010) 1–16.
[67] R.J. Cogdell, A.T. Gardiner, Functions of carotenoids in photosynthesis, Methods Enzymol. 214 (1993) 185–193.
[68] H.A. Frank, R.J. Cogdell, Carotenoids in photosynthesis, Photochem. Photobiol. 63 (1996) 257–264.
[69] N.E. Holt, G.R. Fleming, K.K. Niyogi, Toward an understanding of the mechanism of nonphotochemical quenching in green plants, Biochemistry 43 (2004) 8281–8289.
[70] H.A. Frank, G.W. Brudvig, Redox functions of carotenoids in photosynthesis, Biochemistry 43 (2004) 8607–8615.

[71] O. Sozer, M. Kis, Z. Gombos, B. Ughy, Proteins, glycerolipids and carotenoids in the functional photosystem II architecture, Front. Biosci. 16 (2011) 619–643.
[72] I. Sakurai, J.R. Shen, J. Leng, S. Ohashi, M. Kobayashi, H. Wada, Lipids in oxygen-evolving photosystem II complexes of cyanobacteria and higher plants, J. Biochem. 140 (2006) 201–209.
[73] L.X. Shi, W.P. Schröder, The low molecular mass subunits of the photosynthetic supracomplex, photosystem II, Biochim. Biophys. Acta 1608 (2004) 75–96.
[74] L.E. Thornton, J.L. Roose, H.B. Pakrasi, M. Ikeuchi, The low molecular weight proteins of photosystem II, in: T. Wydrzynski, K. Satoh (Eds.), Photosystem II: The Light-Driven Water:Plastoquinone Oxidoreductase, Springer, Dordrecht, 2005, pp. 121–137.
[75] F.K. Bentley, H. Luo, P. Dilbeck, R.L. Burnap, J.J. Eaton-Rye, Effects of inactivating *psbM* and *psbT* on photodamage and assembly of photosystem II in *Synechocystis* sp. PCC 6803, Biochemistry 47 (2008) 11637–11646.
[76] K. Kawakami, Y. Umena, M. Iwai, Y. Kawabata, M. Ikeuchi, N. Kamiya, J.R. Shen, Roles of PsbI and PsbM in photosystem II dimer formation and stability studied by deletion mutagenesis and X-ray crystallography, Biochim. Biophys. Acta 1807 (2011) 319–325.
[77] J.L. Roose, K.M. Wegener, H.B. Pakrasi, The extrinsic proteins of photosystem II, Photosynth. Res. 92 (2007) 369–387.
[78] I. Enami, A. Okumura, R. Nagao, T. Suzuki, M. Iwai, J.R. Shen, Structures and functions of the extrinsic proteins of photosystem II from different species, Photosynth. Res. 98 (2008) 349–363.
[79] B.R. Green, W.W. Parson, Light-harvesting antennas in photosynthesis, in: Govindjee (Ed.), Advances in Phothosynthesis and Respiration, Springer (Kluwer Academic Publishers), Dordrecht, The Netherlands, 2003.
[80] H. van Amerongen, R. Croce, Structure and function of photosystem II light-harvesting proteins (Lhcb) of higher plants, in: G. Renger (Ed.), Primary Processes of Photosynthesis, Principles and Apparatus, RSC Publishing, Cambridge, U. K., 2008, pp. 329–367.
[81] K. Broess, G. Trinkunas, A. van Hoek, R. Croce, H. van Amerongen, Determination of the excitation migration time in photosystem II — consequences for the membrane organization and charge separation parameters, Biochim. Biophys. Acta 1777 (2008) 404–409.
[82] G. Raszewski, T. Renger, Light harvesting in photosystem II core complexes is limited by the transfer to the trap: can the core complex turn into a photoprotective mode? J. Am. Chem. Soc. 130 (2008) 4431–4446.
[83] T. Renger, E. Schlodder, Primary photophysical processes in photosystem II: bridging the gap between crystal structure and optical spectra, ChemPhysChem 11 (2010) 1141–1153.
[84] Y. Miloslavina, M. Szczepaniak, M.G. Müller, J. Sander, M. Nowaczyk, M. Rögner, A.R. Holzwarth, Charge separation kinetics in intact photosystem II core particles is trap-limited. A picosecond fluorescence study, Biochemistry 45 (2006) 2436–2442.
[85] G. Tumino, A.P. Casazza, E. Engelmann, F.M. Garlaschi, G. Zucchelli, R.C. Jennings, Fluorescence lifetime spectrum of the plant photosystem II core complex: photochemistry does not induce specific reaction center quenching, Biochemistry 47 (2008) 10449–10457.
[86] W. Zinth, J. Wachtveitl, The first picoseconds in bacterial photosynthesis — ultrafast electron transfer for the efficient conversion of light energy, ChemPhysChem 6 (2005) 871–880.
[87] M.E. Madjet, F. Müh, T. Renger, Deciphering the influence of short-range electronic couplings on optical properties of molecular dimers: application to “special pairs” in photosynthesis, J. Phys. Chem. B 113 (2009) 12603–12614.
[88] F. Rappaport, B.A. Diner, Primary photochemistry and energetics leading to the oxidation of the (Mn)4Ca cluster and to the evolution of molecular oxygen in photosystem II, Coord. Chem. Rev. 252 (2008) 259–272.
[89] M. Brecht, V. Radics, J.B. Nieder, R. Bittl, Protein dynamics-induced variation of excitation energy transfer pathways, Proc. Natl. Acad. Sci. U.S.A. 106 (2009) 11857–11861.
[90] E. Romero, I.H.M. van Stokkum, V.I. Novoderezhkin, J.P. Dekker, R. van Grondelle, Two different charge separation pathways in photosystem II, Biochemistry 49 (2010) 4300–4307.
[91] H. Pettai, V. Oja, A. Freiberg, A. Laisk, The long-wavelength limit of plant photosynthesis, FEBS Lett. 579 (2005) 4017–4019.
[92] J.L. Hughes, P. Smith, R. Pace, E. Krausz, Charge separation in photosystem II core complexes induced by 690–730 nm excitation at 1.7 K, Biochim. Biophys. Acta 1757 (2006) 841–851.
[93] A. Thapper, F. Mamedov, F. Mokvist, L. Hammarström, S. Styring, Defining the far-red limit of photosystem II in spinach, Plant Cell 21 (2009) 2391–2401.
[94] I. Ikegami, S. Katoh, Studies on chlorophyll fluorescence in chloroplasts. 2. Effect of ferricyanide on induction of fluorescence in presence of 3-(3,4-dichlorophenyl)-1,1-dimethylurea, Plant Cell Physiol. 14 (1973) 829–836.
[95] J.M. Bowes, A.R. Crofts, S. Itoh, A high potential acceptor for photosystem II, Biochim. Biophys. Acta 547 (1979) 320–335.
[96] V. Petrouleas, B.A. Diner, Identification of $Q_{400}$, a high-potential electron acceptor of photosystem II, with the iron of the quinone–iron acceptor complex, Biochim. Biophys. Acta 849 (1986) 264–275.
[97] H. Ishikita, E.W. Knapp, Oxidation of the non-heme iron complex in photosystem II, Biochemistry 44 (2005) 14772–14783.
[98] J.L. Zimmermann, A.W. Rutherford, Photoreductant-induced oxidation of $Fe^{2+}$ in the electron–acceptor complex of photosystem II, Biochim. Biophys. Acta 851 (1986) 416–423.
[99] V. Petrouleas, B.A. Diner, Light-induced oxidation of the acceptor-side Fe(II) of photosystem II by exogenous quinones acting through the $Q_B$ binding site. 1. Quinones, kinetics and pH-dependence, Biochim. Biophys. Acta 893 (1987) 126–137.
[100] J.J.S. van Rensen, C.H. Xu, Govindjee, Role of bicarbonate in photosystem II, the water-plastoquinone oxido-reductase of plant photosynthesis, Physiol. Plant. 105 (1999) 585–592.
[101] A. Stemler, J.B. Murphy, Bicarbonate-reversible and irreversible inhibition of photosystem II by mono-valent anions, Plant Physiol. 77 (1985) 974–977.
[102] V. Petrouleas, B.A. Diner, Formation by NO of nitrosyl adducts of redox components of the photosystem II reaction center. I. NO binds to the acceptor-side non-heme iron, Biochim. Biophys. Acta 1015 (1990) 131–140.
[103] B.A. Diner, V. Petrouleas, Formation by NO of nitrosyl adducts of redox components of the photosystem II reaction center. II. Evidence that $HCO_3^-/CO_2$ binds to the acceptor-side non-heme iron, Biochim. Biophys. Acta 1015 (1990) 141–149.
[104] R. Hienerwadel, C. Berthomieu, Bicarbonate binding to the non-heme iron of photosystem II investigated by Fourier transform infrared difference spectroscopy and $^{13}C$-labeled bicarbonate, Biochemistry 34 (1995) 16288–16297.
[105] B.A. Diner, V. Petrouleas, J.J. Wendoloski, The iron–quinone electron–acceptor complex of photosystem II, Physiol. Plant. 81 (1991) 423–436.
[106] V. Petrouleas, A.R. Crofts, The iron–quinone acceptor complex, in: T. Wydrzynski, K. Satoh (Eds.), Photosystem II: The Light-Driven Water:Plastoquinone Oxido-reductase, Springer, Dordrecht, 2005, pp. 177–206.
[107] H. Bauwe, M. Hagemann, A.R. Fernie, Photorespiration: players, partners and origin, Trends Plant Sci. 15 (2010) 330–336.
[108] B.A. Diner, V. Petrouleas, $Q_{400}$, the non-heme iron of the photosystem II iron–quinone complex — a spectroscopic probe of quinone and inhibitor binding to the reaction center, Biochim. Biophys. Acta 895 (1987) 107–125.
[109] A.F. Pinto, J.V. Rodrigues, M. Teixeira, Reductive elimination of superoxide: structure and mechanism of superoxide reductases, Biochim. Biophys. Acta 1804 (2010) 285–297.
[110] P. Pospísil, Production of reactive oxygen species by photosystem II, Biochim. Biophys. Acta 1787 (2009) 1151–1160.
[111] P. Pospisil, A. Arato, A. Krieger-Liszkay, A.W. Rutherford, Hydroxyl radical generation by photosystem II, Biochemistry 43 (2004) 6783–6792.
[112] J. Deisenhofer, O. Epp, I. Sinning, H. Michel, Crystallographic refinement at 2.3 Å resolution and refined model of the photosynthetic reaction centre from *Rhodopseudomonas viridis*, J. Mol. Biol. 246 (1995) 429–457.
[113] C.R.D. Lancaster, Structure of reaction centers in anoxygenic bacteria, in: G. Renger (Ed.), Primary Processes of Photosynthesis, Principles and Apparatus, RSC Publishing, Cambridge, 2008, pp. 5–56.
[114] M.L. Waters, Aromatic interactions in model systems, Curr. Opin. Chem. Biol. 6 (2002) 736–741.
[115] C. Kirmaier, D. Holten, W.W. Parson, Temperature and detection-wavelength dependence of the picosecond electron-transfer kinetics measured in *Rhodopseudomonas sphaeroides* reaction centers — resolution of new spectral and kinetic components in the primary charge-separation process, Biochim. Biophys. Acta 810 (1985) 33–48.
[116] A.M. Nuijs, H.J. van Gorkom, J.J. Plijter, L.N.M. Duysens, Primary charge separation and excitation of chlorophyll *a* in photosystem II particles from spinach as studied by picosecond absorbance-difference spectroscopy, Biochim. Biophys. Acta 848 (1986) 167–175.
[117] G.H. Schatz, H. Brock, A.R. Holzwarth, Picosecond kinetics of fluorescence and absorbence changes in photosystem II particles excited at low photon density, Proc. Natl. Acad. Sci. U.S.A. 84 (1987) 8414–8418.
[118] H.J. Eckert, N. Wiese, J. Bernarding, H.J. Eichler, G. Renger, Analysis of the electron transfer from $Pheo^-$ to $Q_A$ in PS II membrane fragments from spinach by time resolved 325 nm absorption changes in the picosecond domain, FEBS Lett. 240 (1988) 153–158.
[119] H.W. Trissl, W. Leibl, Primary charge separation in photosystem II involves two electrogenic steps, FEBS Lett. 244 (1989) 85–88.
[120] J. Bernarding, H.J. Eckert, H.J. Eichler, A. Napiwotzki, G. Renger, Kinetic studies on the stabilization of the primary radical pair $P680^+$ $Pheo^-$ in different photosystem II preparations from higher plants, Photochem. Photobiol. 59 (1994) 566–573.
[121] S. Vasil'ev, A. Bergmann, H. Redlin, H.J. Eichler, G. Renger, On the role of exchangeable hydrogen bonds for the kinetics of $P680^+\bullet Q_A^-\bullet$ formation and $P680^+\bullet Pheo^-\bullet$ recombination in photosystem II, Biochim. Biophys. Acta 1276 (1996) 35–44.
[122] C.A. Wraight, Proton and electron transfer in the acceptor quinone complex of photosynthetic reaction centers from *Rhodobacter sphaeroides*, Front. Biosci. 9 (2004) 309–337.
[123] G. Renger, Functional pattern of photosystem II, in: G. Renger (Ed.), Primary Processes of Photosynthesis, Principles and Apparatus, RSC Publishing, Cambridge, 2008, pp. 237–290.
[124] H.U. Stilz, U. Finkele, W. Holzapfel, C. Lauterwasser, W. Zinth, D. Oesterhelt, Influence of M-subunit Thr222 and Trp252 on quinone binding and electron transfer in *Rhodobacter sphaeroides* reaction centers, Eur. J. Biochem. 223 (1994) 233–242.
[125] M. Plato, M.E. Michel-Beyerle, M. Bixon, J. Jortner, On the role of tryptophan as a superexchange mediator for quinone reduction in photosynthetic reaction centers, FEBS Lett. 249 (1989) 70–74.
[126] I.A. Balabin, J.N. Onuchic, Dynamically controlled protein tunneling paths in photosynthetic reaction centers, Science 290 (2000) 114–117.
[127] H. Nishioka, A. Kimura, T. Yamato, T. Kawatsu, T. Kakitani, Interference, fluctuation, and alternation of electron tunneling in protein media. 1. Two tunneling routes in photosynthetic reaction center alternate due to thermal fluctuation of protein conformation, J. Phys. Chem. B 109 (2005) 1978–1987.
[128] W. Vermaas, J. Charité, G.Z. Shen, $Q_A$ binding to D2 contributes to the functional and structural integrity of photosystem II, Z. Naturforsch. C 45 (1990) 359–365.
[129] R.J. Cogdell, D.C. Brune, R.K. Clayton, Effects of extraction and replacement of ubiquinone upon photochemical activity of reaction centers and chromatophores from *Rhodopseudomonas spheroides*, FEBS Lett. 45 (1974) 344–347.

[130] M.Y. Okamura, R.A. Isaacson, G. Feher, Primary acceptor in bacterial photosynthesis — obligatory role of ubiquinone in photoactive reaction centers of *Rhodopseudomonas spheroides*, Proc. Natl. Acad. Sci. U.S.A. 72 (1975) 3491–3495.

[131] N.W. Woodbury, W.W. Parson, M.R. Gunner, R.C. Prince, P.L. Dutton, Radical-pair energetics and decay mechanisms in reaction centers containing anthraquinones, naphthoquinones or benzoquinones in place of ubiquinone, Biochim. Biophys. Acta 851 (1986) 6–22.

[132] C.A. Wraight, M.R. Gunner, The acceptor quinones of purple photosynthetic bacteria — structure and spectroscopy, in: C.N. Hunter, F. Daldal, M.C. Thurnauer, J.T. Beatty (Eds.), The Purple Phototrophic Bacteria, Springer, Dordrecht, 2009, pp. 379–405.

[133] M.R. Gunner, P.L. Dutton, Temperature and $-\Delta G^0$ dependence of the electron transfer from $Bph^{\bullet -}$ to $Q_A$ in reaction center protein from *Rhodobacter sphaeroides* with different quinones as $Q_A$, J. Am. Chem. Soc. 111 (1989) 3400–3412.

[134] H. Arata, W.W. Parson, Delayed fluorescence from *Rhodopseudomonas sphaeroides* reaction centers — enthalpy and free-energy changes accompanying electron transfer from P-870 to quinones, Biochim. Biophys. Acta 638 (1981) 201–209.

[135] H. Arata, M. Nishimura, Free-energy change accompanying electron transfer from P-870 to quinone in *Rhodopseudomonas sphaeroides* chromatophores, Biochim. Biophys. Acta 725 (1983) 394–401.

[136] K. Turzó, G. Laczkó, Z. Filus, P. Maróti, Quinone-dependent delayed fluorescence from the reaction center of photosynthetic bacteria, Biophys. J. 79 (2000) 14–25.

[137] E. Asztalos, P. Maróti, Export or recombination of charges in reaction centers in intact cells of photosynthetic bacteria, Biochim. Biophys. Acta 1787 (2009) 1444–1450.

[138] H. Cheap, J. Tandori, V. Derrien, M. Benoit, P. de Oliveira, J. Koepke, J. Lavergne, P. Maróti, P. Sebban, Evidence for delocalized anticooperative flash induced proton binding as revealed by mutants at the M266His iron ligand in bacterial reaction centers, Biochemistry 46 (2007) 4510–4521.

[139] R.F. Meiburg, H.J. van Gorkom, R.J. van Dorssen, Excitation trapping and charge separation in photosystem II in the presence of an electrical field, Biochim. Biophys. Acta 724 (1983) 352–358.

[140] F. Rappaport, M. Guergova-Kuras, P.J. Nixon, B.A. Diner, J. Lavergne, Kinetics and pathways of charge recombination in photosystem II, Biochemistry 41 (2002) 8518–8527.

[141] M. Grabolle, H. Dau, Energetics of primary and secondary electron transfer in photosystem II membrane particles of spinach revisited on basis of recombination-fluorescence measurements, Biochim. Biophys. Acta 1708 (2005) 209–218.

[142] J.M. Hou, V.A. Boichenko, B.A. Diner, D. Mauzerall, Thermodynamics of electron transfer in oxygenic photosynthetic reaction centers: volume change, enthalpy, and entropy of electron-transfer reactions in manganese-depleted photosystem II core complexes, Biochemistry 40 (2001) 7117–7125.

[143] R.C. Prince, P.L. Dutton, The primary acceptor of bacterial photosynthesis — its operating midpoint potential? Arch. Biochem. Biophys. 172 (1976) 329–334.

[144] P.H. McPherson, V. Nagarajan, W.W. Parson, M.Y. Okamura, G. Feher, pH-dependence of the free-energy gap between $DQ_A$ and $D^+Q_A^-$ determined from delayed fluorescence in reaction centers from *Rhodobacter sphaeroides* R-26, Biochim. Biophys. Acta 1019 (1990) 91–94.

[145] P. Maróti, C.A. Wraight, Flash-induced $H^+$ binding by bacterial photosynthetic reaction centers — influences of the redox states of the acceptor quinones and primary donor, Biochim. Biophys. Acta 934 (1988) 329–347.

[146] P. Maróti, C.A. Wraight, The redox midpoint potential of the primary quinone of reaction centers in chromatophores of *Rhodobacter sphaeroides* is pH independent, Eur. Biophys. J. 37 (2008) 1207–1217.

[147] A. Krieger, A.W. Rutherford, G.N. Johnson, On the determination of redox midpoint potential of the primary quinone electron acceptor, $Q_A$, in Photosystem II, Biochim. Biophys. Acta 1229 (1995) 193–201.

[148] G.N. Johnson, A.W. Rutherford, A. Krieger, A change in the midpoint potential of the quinone $Q_A$ in photosystem II associated with photoactivation of oxygen evolution, Biochim. Biophys. Acta 1229 (1995) 202–207.

[149] Z.Y. Zhu, M.R. Gunner, Energetics of quinone-dependent electron and proton transfers in *Rhodobacter sphaeroides* photosynthetic reaction centers, Biochemistry 44 (2005) 82–96.

[150] H. Ishikita, E.W. Knapp, Control of quinone redox potentials in photosystem II: electron transfer and photoprotection, J. Am. Chem. Soc. 127 (2005) 14714–14720.

[151] J. Breton, C. Boullais, J.R. Burie, E. Nabedryk, C. Mioskowski, Binding-sites of quinones in photosynthetic bacterial reaction centers investigated by light-induced FTIR difference spectroscopy — assignment of the interactions of each carbonyl of $Q_A$ in *Rhodobacter sphaeroides* using site-specific $^{13}C$-labeled ubiquinone, Biochemistry 33 (1994) 14378–14386.

[152] R. Brudler, H.J.M. de Groot, W.B.S. van Liemt, W.F. Steggerda, R. Esmeijer, P. Gast, A.J. Hoff, J. Lugtenburg, K. Gerwert, Asymmetric binding of the 1- and 4-C=0 Groups of $Q_A$ in *Rhodobacter sphaeroides* R26 reaction centers monitored by Fourier-transform infrared spectroscopy using site-specific isotopically labeled ubiquinone-10, EMBO J. 13 (1994) 5523–5530.

[153] T. Noguchi, Y. Inoue, X.S. Tang, Hydrogen bonding interaction between the primary quinone acceptor $Q_A$ and a histidine side chain in photosystem II as revealed by Fourier transform infrared spectroscopy, Biochemistry 38 (1999) 399–403.

[154] W.F. Butler, R. Calvo, D.R. Fredkin, R.A. Isaacson, M.Y. Okamura, G. Feher, The electronic structure of $Fe^{2+}$ in reaction centers from *Rhodopseudomonas sphaeroides*. III. EPR measurements of the reduced acceptor complex, Biophys. J. 45 (1984) 947–973.

[155] A.W. Rutherford, J.L. Zimmermann, A new EPR signal attributed to the primary plastosemiquinone acceptor in photosystem II, Biochim. Biophys. Acta 767 (1984) 168–175.

[156] J.H.A. Nugent, D.C. Doetschman, D.J. MacLachlan, Characterization of the multiple ESR line shapes of iron semiquinones in photosystem 2, Biochemistry 31 (1992) 2935–2941.

[157] W.F.J. Vermaas, A.W. Rutherford, EPR measurements on the effects of bicarbonate and triazine resistance on the acceptor side of photosystem II, FEBS Lett. 175 (1984) 243–248.

[158] G. Chen, Y. Allahverdiyeva, E.M. Aro, S. Styring, F. Mamedov, Electron paramagnetic resonance study of the electron transfer reactions in photosystem II membrane preparations from *Arabidopsis thaliana*, Biochim. Biophys. Acta 1807 (2011) 205–215.

[159] N. Cox, L. Jin, A. Jaszewski, P.J. Smith, E. Krausz, A.W. Rutherford, R. Pace, The semiquinone–iron complex of photosystem II: structural insights from ESR and theoretical simulation; evidence that the native ligand to the non-heme iron is carbonate, Biophys. J. 97 (2009) 2024–2033.

[160] R.J. Debus, G. Feher, M.Y. Okamura, Iron-depleted reaction centers from *Rhodopseudomonas sphaeroides* R-26.1 — characterization and reconstitution with $Fe^{2+}$, $Mn^{2+}$, $Co^{2+}$, $Ni^{2+}$, $Cu^{2+}$, and $Zn^{2+}$, Biochemistry 25 (1986) 2276–2287.

[161] L.M. Utschig, S.R. Greenfield, J. Tang, P.D. Laible, M.C. Thurnauer, Influence of iron-removal procedures on sequential electron transfer in photosynthetic bacterial reaction centers studied by transient EPR spectroscopy, Biochemistry 36 (1997) 8548–8558.

[162] B. Arnoux, J.F. Gaucher, A. Ducruix, F. Reiss-Husson, Structure of the photochemical reaction center of a spheroidene-containing purple bacterium, *Rhodobacter sphaeroides* Y, at 3 Å resolution, Acta Crystallogr. D 51 (1995) 368–379.

[163] W. Lubitz, G. Feher, The primary and secondary acceptors in bacterial photosynthesis III. Characterization of the quinone radicals $Q_A^-\bullet$ and $Q_B^-\bullet$ by EPR and ENDOR, Appl. Magn. Reson. 17 (1999) 1–48.

[164] D. Kleinfeld, M.Y. Okamura, G. Feher, Electron transfer kinetics in photosynthetic reaction centers cooled to cryogenic temperatures in the charge-separated state — evidence for light-induced structural changes, Biochemistry 23 (1984) 5780–5786.

[165] S.G. Zech, R. Bittl, A.T. Gardiner, W. Lubitz, Transient and pulsed EPR spectroscopy on the radical pair state $P_{865}^+\bullet Q_A^-\bullet$ to study light-induced changes in bacterial reaction centers, Appl. Magn. Reson. 13 (1997) 517–529.

[166] E.C. Abresch, A.P. Yeh, S.M. Soltis, D.C. Rees, H.L. Axelrod, M.Y. Okamura, G. Feher, Crystal structure of the charge-separated state, $D^+Q_A^-$ in photosynthetic reaction centers from *Rb. sphaeroides*, Biophys. J. 76 (1999) A141.

[167] G. Katona, A. Snijder, P. Gourdon, U. Andréasson, Ö. Hansson, L.E. Andréasson, R. Neutze, Conformational regulation of charge recombination reactions in a photosynthetic bacterial reaction center, Nat. Struct. Mol. Biol. 12 (2005) 630–631.

[168] M. Flores, A. Savitsky, M.L. Paddock, E.C. Abresch, A.A. Dubinskii, M.Y. Okamura, W. Lubitz, K. Möbius, Electron–nuclear and electron–electron double resonance spectroscopies show that the primary quinone acceptor $Q_A$ in reaction centers from photosynthetic bacteria *Rhodobacter sphaeroides* remains in the same orientation upon light-induced reduction, J. Phys. Chem. B 114 (2010) 16894–16901.

[169] A.V. Astashkin, H. Hara, S. Kuroiwa, A. Kawamori, K. Akabori, A comparative electron spin echo envelope modulation study of the primary electron acceptor quinone in Zn-substituted and cyanide-treated preparations of photosystem II, J. Chem. Phys. 108 (1998) 10143–10151.

[170] J.M. Peloquin, X.S. Tang, B.A. Diner, R.D. Britt, An electron spin-echo envelope modulation (ESEEM) study of the $Q_A$ binding pocket of PS II reaction centers from spinach and *Synechocystis*, Biochemistry 38 (1999) 2057–2067.

[171] F. MacMillan, F. Lendzian, G. Renger, W. Lubitz, EPR and ENDOR investigation of the primary electron acceptor radical anion $Q_A\bullet^-$ in iron-depleted photosystem II membrane fragments, Biochemistry 34 (1995) 8144–8156.

[172] R. Chatterjee, S. Milikisiyants, C.S. Coates, K.V. Lakshmi, High-resolution two-dimensional $^1H$ and $^{14}N$ hyperfine sublevel correlation spectroscopy of the primary quinone of photosystem II, Biochemistry 50 (2011) 491–501.

[173] Y. Deligiannakis, C. Jegerschöld, A.W. Rutherford, EPR and ESEEM study of the plastoquinone anion radical $Q_A^-\bullet$ in photosystem II treated at high pH, Chem. Phys. Lett. 270 (1997) 564–572.

[174] T. Noguchi, J. Kurreck, Y. Inoue, G. Renger, Comparative FTIR analysis of the microenvironment of $Q_A^-\bullet$ in cyanide-treated, high pH-treated and iron-depleted photosystem II membrane fragments, Biochemistry 38 (1999) 4846–4852.

[175] C.H. Chang, O. El-Kabbani, D. Tiede, J. Norris, M. Schiffer, Structure of the membrane-bound protein photosynthetic reaction center from *Rhodobacter sphaeroides*, Biochemistry 30 (1991) 5352–5360.

[176] O. El-Kabbani, C.H. Chang, D. Tiede, J. Norris, M. Schiffer, Comparison of reaction centers from *Rhodobacter sphaeroides* and *Rhodopseudomonas viridis* — overall architecture and protein–pigment interactions, Biochemistry 30 (1991) 5361–5369.

[177] U. Ermler, G. Fritzsch, S.K. Buchanan, H. Michel, Structure of the photosynthetic reaction centre from *Rhodobacter sphaeroides* at 2.65 Å resolution — cofactors and protein–cofactor interactions, Structure 2 (1994) 925–936.

[178] M.H.B. Stowell, T.M. McPhillips, D.C. Rees, S.M. Soltis, E. Abresch, G. Feher, Light-induced structural changes in photosynthetic reaction center: implications for mechanism of electron–proton transfer, Science 276 (1997) 812–816.

[179] R.H. Baxter, N. Ponomarenko, V. Srajer, R. Pahl, K. Moffat, J.R. Norris, Time-resolved crystallographic studies of light-induced structural changes in the photosynthetic reaction center, Proc. Natl. Acad. Sci. U.S.A. 101 (2004) 5982–5987.

[180] R.H. Baxter, B.L. Seagle, N. Ponomarenko, J.R. Norris, Cryogenic structure of the photosynthetic reaction center of *Blastochloris viridis* in the light and dark, Acta Crystallogr. D 61 (2005) 605–612.

[181] P.R. Pokkuluri, P.D. Laible, A.E. Crawford, J.F. Mayfield, M.A. Yousef, S.L. Ginell, D.K. Hanson, M. Schiffer, Temperature and cryoprotectant influence secondary

quinone binding position in bacterial reaction centers, FEBS Lett. 570 (2004) 171–174.
[182] C. Fufezan, C.X. Zhang, A. Krieger-Liszkay, A.W. Rutherford, Secondary quinone in photosystem II of *Thermosynechococcus elongatus*: semiquinone–iron EPR signals and temperature dependence of electron transfer, Biochemistry 44 (2005) 12780–12789.
[183] R. Krivanek, J. Kern, A. Zouni, H. Dau, M. Haumann, Spare quinones in the $Q_B$ cavity of crystallized photosystem II from *Thermosynechococcus elongatus*, Biochim. Biophys. Acta 1767 (2007) 520–527.
[184] I. Sinning, H. Michel, P. Mathis, A.W. Rutherford, Characterization of four herbicide-resistant mutants of *Rhodopseudomonas viridis* by genetic analysis, electron paramagnetic resonance, and optical spectroscopy, Biochemistry 28 (1989) 5544–5553.
[185] G. Fritzsch, J. Koepke, R. Diem, A. Kuglstatter, L. Baciou, Charge separation induces conformational changes in the photosynthetic reaction centre of purple bacteria, Acta Crystallogr. D 58 (2002) 1660–1663.
[186] J. Breton, C. Boullais, G. Berger, C. Mioskowski, E. Nabedryk, Binding-sites of quinones in photosynthetic bacterial reaction centers investigated by light-induced FTIR difference spectroscopy — symmetry of the carbonyl interactions and close equivalence of the $Q_B$ vibrations in *Rhodobacter sphaeroides* and *Rhodopseudomonas viridis* probed by isotope labeling, Biochemistry 34 (1995) 11606–11616.
[187] J. Breton, C. Boullais, C. Mioskowski, P. Sebban, L. Baciou, E. Nabedryk, Vibrational spectroscopy favors a unique $Q_B$ binding site at the proximal position in wild-type reaction centers and in the Pro-L209→Tyr mutant from *Rhodobacter sphaeroides*, Biochemistry 41 (2002) 12921–12927.
[188] J. Breton, Absence of large-scale displacement of quinone $Q_B$ in bacterial photosynthetic reaction centers, Biochemistry 43 (2004) 3318–3326.
[189] R. Brudler, H.J.M. de Groot, W.B.S. van Liemt, P. Gast, A.J. Hoff, J. Lugtenburg, K. Gerwert, FTIR spectroscopy shows weak symmetrical hydrogen bonding of the $Q_B$ carbonyl groups in *Rhodobacter sphaeroides* R26 reaction centers, FEBS Lett. 370 (1995) 88–92.
[190] E. Nabedryk, J. Breton, Coupling of electron transfer to proton uptake at the $Q_B$ site of the bacterial reaction center: a perspective from FTIR difference spectroscopy, Biochim. Biophys. Acta 1777 (2008) 1229–1248.
[191] H. Suzuki, M. Nagasaka, M. Sugiura, T. Noguchi, Fourier transform infrared spectrum of the secondary quinone electron acceptor $Q_B$ in photosystem II, Biochemistry 44 (2005) 11323–11328.
[192] M.Y. Okamura, M.L. Paddock, M.S. Graige, G. Feher, Proton and electron transfer in bacterial reaction centers, Biochim. Biophys. Acta 1458 (2000) 148–163.
[193] M.L. Paddock, G. Feher, M.Y. Okamura, Proton transfer pathways and mechanism in bacterial reaction centers, FEBS Lett. 555 (2003) 45–50.
[194] H. Cheap, S. Bernad, V. Derrien, L. Gerencsér, J. Tandori, P. de Oliveira, D.K. Hanson, P. Maróti, P. Sebban, M234Glu is a component of the proton sponge in the reaction center from photosynthetic bacteria, Biochim. Biophys. Acta 1787 (2009) 1505–1515.
[195] P. Beroza, D.R. Fredkin, M.Y. Okamura, G. Feher, Electrostatic calculations of amino acid titration and electron transfer, $Q_A^-Q_B \rightarrow Q_AQ_B^-$, in the reaction center, Biophys. J. 68 (1995) 2233–2250.
[196] C.R.D. Lancaster, H. Michel, B. Honig, M.R. Gunner, Calculated coupling of electron and proton transfer in the photosynthetic reaction center of *Rhodopseudomonas viridis*, Biophys. J. 70 (1996) 2469–2492.
[197] B. Rabenstein, G.M. Ullmann, E.W. Knapp, Electron transfer between the quinones in the photosynthetic reaction center and its coupling to conformational changes, Biochemistry 39 (2000) 10487–10496.
[198] H. Ishikita, G. Morra, E.W. Knapp, Redox potential of quinones in photosynthetic reaction centers from *Rhodobacter sphaeroides*: dependence on protonation of Glu-L212 and Asp-L213, Biochemistry 42 (2003) 3882–3892.
[199] M.L. Paddock, M. Flores, R. Isaacson, C. Chang, E.C. Abresch, M.Y. Okamura, ENDOR spectroscopy reveals light induced movement of the H-bond from Ser-L223 upon forming the semiquinone ($Q_B^{-*}$) in reaction centers from *Rhodobacter sphaeroides*, Biochemistry 46 (2007) 8234–8243.
[200] E. Nabedryk, M.L. Paddock, M.Y. Okamura, J. Breton, An isotope-edited FTIR investigation of the role of Ser-L223 in binding quinone ($Q_B$) and serniquinone ($Q_B^-$) in the reaction center from *Rhodobacter sphaeroides*, Biochemistry 44 (2005) 14519–14527.
[201] F. Francia, G. Palazzo, A. Mallardi, L. Cordone, G. Venturoli, Residual water modulates $Q_A^-$ to $Q_B$ electron transfer in bacterial reaction centers embedded in trehalose amorphous matrices, Biophys. J. 85 (2003) 2760–2775.
[202] G. Palazzo, F. Francia, A. Mallardi, M. Giustini, F. Lopez, G. Venturoli, Water activity regulates the $Q_A^-$ to $Q_B$ electron transfer in photosynthetic reaction centers from *Rhodobacter sphaeroides*, J. Am. Chem. Soc. 130 (2008) 9353–9363.
[203] M.S. Graige, G. Feher, M.Y. Okamura, Conformational gating of the electron transfer reaction $Q_A^-{}^*Q_B \rightarrow Q_AQ_B^{-*}$ in bacterial reaction centers of *Rhodobacter sphaeroides* determined by a driving force assay, Proc. Natl. Acad. Sci. U.S.A. 95 (1998) 11679–11684.
[204] J.L. Li, E. Takahashi, M.R. Gunner, $-\Delta G^0_{AB}$ and pH dependence of the electron transfer from $P^+Q_A^-Q_B$ to $P^+Q_AQ_B^-$ in *Rhodobacter sphaeroides* reaction centers, Biochemistry 39 (2000) 7445–7454.
[205] A. Kuglstatter, U. Ermler, H. Michel, L. Baciou, G. Fritzsch, X-ray structure analyses of photosynthetic reaction center variants from *Rhodobacter sphaeroides*: structural changes induced by point mutations at position L209 modulate electron and proton transfer, Biochemistry 40 (2001) 4253–4260.
[206] J. Tandori, P. Maróti, E. Alexov, P. Sebban, L. Baciou, Key role of proline L209 in connecting the distant quinone pockets in the reaction center of *Rhodobacter sphaeroides*, Proc. Natl. Acad. Sci. U.S.A. 99 (2002) 6702–6706.
[207] A. Remy, K. Gerwert, Coupling of light-induced electron transfer to proton uptake in photosynthesis, Nat. Struct. Biol. 10 (2003) 637–644.
[208] S. Hermes, O. Bremm, F. Garczarek, V. Derrien, P. Liebisch, P. Loja, P. Sebban, K. Gerwert, M. Haumann, A time-resolved iron-specific X-ray absorption experiment yields no evidence for an $Fe^{2+} \rightarrow Fe^{3+}$ transition during $Q_A^- \rightarrow Q_B$ electron transfer in the photosynthetic reaction center, Biochemistry 45 (2006) 353–359.
[209] J. Breton, Steady-state FTIR spectra of the photoreduction of $Q_A$ and $Q_B$ in *Rhodobacter sphaeroides* reaction centers provide evidence against the presence of a proposed transient electron acceptor X between the two quinones, Biochemistry 46 (2007) 4459–4465.
[210] R. de Wijn, H.J. van Gorkom, Kinetics of electron transfer from $Q_A$ to $Q_B$ in photosystem II, Biochemistry 40 (2001) 11912–11922.
[211] W.F.J. Vermaas, G. Renger, G. Dohnt, The reduction of the oxygen-evolving system in chloroplasts by thylakoid components, Biochim. Biophys. Acta 764 (1984) 194–202.
[212] A.W. Rutherford, G. Renger, H. Koike, Y. Inoue, Thermo-luminescence as a probe of photosystem II — the redox and protonation states of the secondary acceptor quinone and the $O_2$-evolving enzyme, Biochim. Biophys. Acta 767 (1984) 548–556.
[213] R. de Wijn, T. Schrama, H.J. van Gorkom, Secondary stabilization reactions and proton-coupled electron transport in photosystem II investigated by electroluminescence and fluorescence spectroscopy, Biochemistry 40 (2001) 5821–5834.
[214] G. Renger, H.J. Eckert, A. Bergmann, J. Bernarding, B. Liu, A. Napiwotzki, F. Reifarth, H.J. Eichler, Fluorescence and spectroscopic studies of exciton trapping and electron-transfer in photosystem II of higher plants, Aust. J. Plant Physiol. 22 (1995) 167–181.
[215] O. Kaminskaya, G. Renger, V.A. Shuvalov, Effect of dehydration on light-induced reactions in photosystem II: photoreactions of cytochrome *b*559, Biochemistry 42 (2003) 8119–8132.
[216] J. Pieper, T. Hauss, A. Buchsteiner, K. Baczynski, K. Adamiak, R.E. Lechner, G. Renger, Temperature- and hydration-dependent protein dynamics in photosystem II of green plants studied by quasielastic neutron scattering, Biochemistry 46 (2007) 11398–11409.
[217] A. Garbers, F. Reifarth, J. Kurreck, G. Renger, F. Parak, Correlation between protein flexibility and electron transfer from $Q_A^-$ to $Q_B$ in PSII membrane fragments from spinach, Biochemistry 37 (1998) 11399–11404.
[218] C.C. Moser, C.C. Page, P.L. Dutton, Tunneling in PSII, Photochem. Photobiol. Sci. 4 (2005) 933–939.
[219] M.S. Graige, M.L. Paddock, J.M. Bruce, G. Feher, M.Y. Okamura, Mechanism of proton-coupled electron transfer for quinone ($Q_B$) reduction in reaction centers of *Rb. sphaeroides*, J. Am. Chem. Soc. 118 (1996) 9005–9016.
[220] M.S. Graige, M.L. Paddock, G. Feher, M.Y. Okamura, Observation of the protonated semiquinone intermediate in isolated reaction centers from *Rhodobacter sphaeroides*: implications for the mechanism of electron and proton transfer in proteins, Biochemistry 38 (1999) 11465–11473.
[221] M.S. Graige, M.L. Paddock, G. Feher, M.Y. Okamura, The mechanism of proton-coupled electron transfer in mutant RCs from *Rb. sphaeroides*, Biophys. J. 74 (1998) A135.
[222] M. Haumann, W. Junge, The rates of proton uptake and electron transfer at the reducing side of photosystem II in thylakoids, FEBS Lett. 347 (1994) 45–50.
[223] M.L. Paddock, S.H. Rongey, G. Feher, M.Y. Okamura, Pathway of proton transfer in bacterial reaction centers: replacement of glutamic acid 212 in the L subunit by glutamine inhibits quinone (secondary acceptor) turnover, Proc. Natl. Acad. Sci. U.S.A. 86 (1989) 6602–6606.
[224] P.H. McPherson, M. Schönfeld, M.L. Paddock, M.Y. Okamura, G. Feher, Protonation and free energy changes associated with formation of QBH2 in native and Glu-L212→Gln mutant reaction centers from *Rhodobacter sphaeroides*, Biochemistry 33 (1994) 1181–1193.
[225] J.J.S. van Rensen, W.J.M. Tonk, S.M. Debruijn, Involvement of bicarbonate in the protonation of the secondary quinone electron acceptor of photosystem II via the non-heme iron of the quinone–iron acceptor complex, FEBS Lett. 226 (1988) 347–351.
[226] J. Kern, A. Zouni, A. Guskov, N. Krauss, Lipids in the structure of photosystem I, photosystem II, and the cytochrome $b_6f$ complex, in: H. Wada, N. Murata (Eds.), Lipids in Photosynthesis, Essential and Regulatory Functions, Springer, Dordrecht, 2009, pp. 203–242.
[227] B. Nowicka, J. Kruk, Occurrence, biosynthesis and function of isoprenoid quinones, Biochim. Biophys. Acta 1797 (2010) 1587–1605.
[228] P.A. Siegenthaler, N. Murata, Lipids in Photosynthesis, Kluwer, Dordrecht, 1998.
[229] H. Wada, N. Murata, Lipids in Photosynthesis, Essential and Regulatory Functions, Springer, Dordrecht, 2009.
[230] N. Sato, M. Hagio, H. Wada, M. Tsuzuki, Requirement of phosphatidylglycerol for photosynthetic function in thylakoid membranes, Proc. Natl. Acad. Sci. U.S.A. 97 (2000) 10655–10660.
[231] M. Hagio, I. Sakurai, S. Sato, T. Kato, S. Tabata, H. Wada, Phosphatidylglycerol is essential for the development of thylakoid membranes in *Arabidopsis thaliana*, Plant Cell Physiol. 43 (2002) 1456–1464.
[232] H. Wada, N. Murata, The essential role of phosphatidylglycerol in photosynthesis, Photosynth. Res. 92 (2007) 205–215.
[233] N. Sato, Roles of the acidic lipids sulfoquinovosyl diacylglycerol and phosphatidylglycerol in photosynthesis: their specificity and evolution, J. Plant Res. 117 (2004) 495–505.
[234] J. Leng, I. Sakurai, H. Wada, J.R. Shen, Effects of phospholipase and lipase treatments on photosystem II core dimer from a thermophilic cyanobacterium, Photosynth. Res. 98 (2008) 469–478.
[235] E.H. Kim, R. Razeghifard, J.M. Anderson, W.S. Chow, Multiple sites of retardation of electron transfer in photosystem II after hydrolysis of phosphatidylglycerol, Photosynth. Res. 93 (2007) 149–158.

[236] Z. Gombos, Z. Varkonyi, M. Hagio, M. Iwaki, L. Kovacs, K. Masamoto, S. Itoh, H. Wada, Phosphatidylglycerol requirement for the function of electron acceptor plastoquinone $Q_B$ in the photosystem II reaction center, Biochemistry 41 (2002) 3796–3802.
[237] M.R. Jones, Lipids in photosynthetic reaction centres: structural roles and functional holes, Prog. Lipid Res. 46 (2007) 56–87.
[238] R.G. Herrmann, J. Alt, B. Schiller, W.R. Widger, W.A. Cramer, Nucleotide-sequence of the gene for apocytochrome *b*-559 on the spinach plastid chromosome — implications for the structure of the membrane protein, FEBS Lett. 176 (1984) 239–244.
[239] W.R. Widger, W.A. Cramer, M. Hermodson, R.G. Herrmann, Evidence for a hetero-oligomeric structure of the chloroplast cytochrome *b*-559, FEBS Lett. 191 (1985) 186–190.
[240] G.T. Babcock, W.R. Widger, W.A. Cramer, W.A. Oertling, J.G. Metz, Axial ligands of chloroplast cytochrome *b*-559: identification and requirement for a heme-cross-linked polypeptide structure, Biochemistry 24 (1985) 3638–3645.
[241] G.S. Tae, M.T. Black, W.A. Cramer, O. Vallon, L. Bogorad, Thylakoid membrane protein topography: transmembrane orientation of the chloroplast cytochrome *b*-559 *psbE* gene product, Biochemistry 27 (1988) 9075–9080.
[242] G.S. Tae, W.A. Cramer, Lumen-side topography of the alpha-subunit of the chloroplast cytochrome *b*-559, FEBS Lett. 259 (1989) 161–164.
[243] J. Bergström, T. Vänngard, EPR signals and orientation of cytochromes in the spinach chloroplast thylakoid membrane, Biochim. Biophys. Acta 682 (1982) 452–456.
[244] K. Burda, J. Kruk, R. Borgstädt, J. Stanek, K. Strzalka, G.H. Schmid, O. Kruse, Mössbauer studies of the non-heme iron and cytochrome *b*559 in a *Chlamydomonas reinhardtii* $PSI^-$ mutant and their interactions with α-tocopherol quinone, FEBS Lett. 535 (2003) 159–165.
[245] R. Fiege, V.A. Shuvalov, Correlated behavior of the EPR signal of cytochrome *b*-559 heme Fe(III) ligated by OH— and the multiline signal of the Mn cluster in PS-II membrane fragments, FEBS Lett. 387 (1996) 33–35.
[246] O. Kaminskaya, J. Kurreck, K.D. Irrgang, G. Renger, V.A. Shuvalov, Redox and spectral properties of cytochrome $b_{559}$ in different preparations of photosystem II, Biochemistry 38 (1999) 16223–16235.
[247] G.S. Tae, W.A. Cramer, Topography of the heme prosthetic group of cytochrome *b*-559 in the photosystem II reaction center, Biochemistry 33 (1994) 10060–10068.
[248] J. Kruk, K. Strzalka, Redox changes of cytochrome *b*(559) in the presence of plastoquinones, J. Biol. Chem. 276 (2001) 86–91.
[249] O. Kaminskaya, V.A. Shuvalov, G. Renger, Evidence for a novel quinone-binding site in the photosystem II (PS II) complex that regulates the redox potential of cytochrome *b*559, Biochemistry 46 (2007) 1091–1105.
[250] J. Whitmarsh, H.B. Pakrasi, Form and function of cytochrome *b*-559, in: D.R. Ort, C.F. Yocum (Eds.), Oxygenic Photosynthesis: The Light Reactions, Kluwer, Dordrecht, 1996, pp. 249–264.
[251] D.H. Stewart, G.W. Brudvig, Cytochrome *b*559 of photosystem II, Biochim. Biophys. Acta 1367 (1998) 63–87.
[252] P. Faller, C. Fufezan, A.W. Rutherford, Side-path electron donors: cytochrome $b_{559}$, chlorophyll Z and β-carotene, in: T. Wydrzynski, K. Satoh (Eds.), Photosystem II: The Light-Driven Water:Plastoquinone Oxidoreductase, Springer, Dordrecht, 2005, pp. 347–365.
[253] J.M. Ortega, M. Hervás, M. Losada, Redox and acid–base characterization of cytochrome *b*-559 in photosystem II particles, Eur. J. Biochem. 171 (1988) 449–455.
[254] L.K. Thompson, A.F. Miller, C.A. Buser, J.C. de Paula, G.W. Brudvig, Characterization of the multiple forms of cytochrome $b_{559}$ in photosystem II, Biochemistry 28 (1989) 8048–8056.
[255] V.A. Shuvalov, U. Schreiber, U. Heber, Spectral and thermodynamic properties of the two hemes of the D1D2cytochrome *b*-559 complex of spinach, FEBS Lett. 337 (1994) 226–230.
[256] V.P. McNamara, K. Gounaris, Granal photosystem II complexes contain only the high redox potential form of cytochrome *b*-559 which is stabilized by the ligation of calcium, Biochim. Biophys. Acta 1231 (1995) 289–296.
[257] I. Iwasaki, N. Tamura, S. Okayama, Effects of light stress on redox potential forms of cyt *b*-559 in photosystem II membranes depleted of water-oxidizing complex, Plant Cell Physiol. 36 (1995) 583–589.
[258] M. Roncel, J.M. Ortega, M. Losada, Factors determining the special redox properties of photosynthetic cytochrome *b*559, Eur. J. Biochem. 268 (2001) 4961–4968.
[259] V.A. Shuvalov, Composition and function of cytochrome *b*559 in reaction centers of photosystem II of green plants, J. Bioenerg. Biomembr. 26 (1994) 619–626.
[260] W.L. Butler, Role of cytochrome *b*559 in oxygen evolution in photosynthesis, FEBS Lett. 95 (1978) 19–25.
[261] A. Desbois, M. Lutz, Redox control of proton transfers in membrane *b*-type cytochromes — an absorption and resonance Raman study on bis(imidazole) and bis(imidazolate) model complexes of iron-protoporphyrin, Eur. Biophys. J. 20 (1992) 321–335.
[262] C. Berthomieu, A. Boussac, W. Mäntele, J. Breton, E. Nabedryk, Molecular changes following oxidoreduction of cytochrome *b*559 characterized by Fourier-transform infrared difference spectroscopy and electron paramagnetic resonance — photooxidation in photosystem II and electrochemistry of isolated cytochrome *b*559 and iron protoporphyrin IX-bisimidazole model compounds, Biochemistry 31 (1992) 11460–11471.
[263] L.I. Krishtalik, G.S. Tae, D.A. Cherepanov, W.A. Cramer, The redox properties of cytochromes *b* imposed by the membrane electrostatic environment, Biophys. J. 65 (1993) 184–195.
[264] W.A. Cramer, J. Whitmarsh, Photosynthetic cytochromes, Annu. Rev. Plant. Physiol. 28 (1977) 133–172.
[265] K. Wada, D.I. Arnon, Three forms of cytochrome $b_{559}$ and their relation to the photosynthetic activity of chloroplasts, Proc. Natl. Acad. Sci. U.S.A. 68 (1971) 3064–3086.
[266] R.P. Cox, D.S. Bendall, Effects on cytochrome $b$-$559_{HP}$ and P546 of treatments that inhibit oxygen evolution by chloroplasts, Biochim. Biophys. Acta 238 (1972) 124–135.
[267] P. Horton, E. Croze, The relationship between activity of chloroplast photosystem II and the midpoint oxidation-reduction potential of cytochrome *b*-559, Biochim. Biophys. Acta 462 (1977) 86–101.
[268] P.R. Rich, D.S. Bendall, The redox potentials of the *b*-type cytochromes of higher plant chloroplasts, Biochim. Biophys. Acta 591 (1980) 153–161.
[269] J.M. Ortega, M. Hervas, M. Losada, Distinctive stability of the reduced and oxidized forms of high-potential cytochrome *b*-559 in photosystem II particles, Plant Sci. 68 (1990) 71–75.
[270] O. Kaminskaya, J. Kern, V.A. Shuvalov, G. Renger, Extinction coefficients of cytochromes *b*559 and *c*550 of *Thermosynechococus elongatus* and cyt *b*559/PS II stoichiometry of higher plants, Biochim. Biophys. Acta 1708 (2005) 333–341.
[271] N. Bondarava, L. de Pascalis, S. Al-Babili, C. Goussias, J.R. Golecki, P. Beyer, R. Bock, A. Krieger-Liszkay, Evidence that cytochrome $b_{559}$ mediates the oxidation of reduced plastoquinone in the dark, J. Biol. Chem. 278 (2003) 13554–13560.
[272] J. Kruk, K. Strzalka, Dark reoxidation of the plastoquinone-pool is mediated by the low-potential form of cytochrome *b*-559 in spinach thylakoids, Photosynth. Res. 62 (1999) 273–279.
[273] A. Tiwari, P. Pospisil, Superoxide oxidase and reductase activity of cytochrome *b*559 in photosystem II, Biochim. Biophys. Acta 1787 (2009) 985–994.
[274] F. Morais, J. Barber, P.J. Nixon, The chloroplast-encoded α subunit of cytochrome *b*-559 is required for assembly of the photosystem two complex in both the light and the dark in *Chlamydomonas reinhardtii*, J. Biol. Chem. 273 (1998) 29315–29320.
[275] F. Morais, K. Kuhn, D.H. Stewart, J. Barber, G.W. Brudvig, P.J. Nixon, Photosynthetic water oxidation in cytochrome *b*559 mutants containing a disrupted heme-binding pocket, J. Biol. Chem. 276 (2001) 31986–31993.
[276] B. Müller, L.A. Eichacker, Assembly of the D1 precursor in monomeric photosystem II reaction center precomplexes precedes chlorophyll *a*-triggered accumulation of reaction center II in barley etioplasts, Plant Cell 11 (1999) 2365–2377.
[277] M. Swiatek, R.E. Regel, J. Meurer, G. Wanner, H.B. Pakrasi, I. Ohad, R.G. Herrmann, Effects of selective inactivation of individual genes for low-molecular-mass subunits on the assembly of photosystem II, as revealed by chloroplast transformation: the *psbEFLJ* operon in *Nicotiana tabacum*, Mol. Genet. Genomics 268 (2003) 699–710.
[278] J. Barber, J. De Las Rivas, A functional model for the role of cytochrome $b_{559}$ in the protection against donor and acceptor side photoinhibition, Proc. Natl. Acad. Sci. U.S.A. 90 (1993) 10942–10946.
[279] S. Styring, A.W. Rutherford, Deactivation kinetics and temperature-dependence of the S-state transitions in the oxygen-evolving system of photosystem II measured by EPR spectroscopy, Biochim. Biophys. Acta 933 (1988) 378–387.
[280] C.X. Zhang, A. Boussac, A.W. Rutherford, Low-temperature electron transfer in photosystem II: a tyrosyl radical and semiquinone charge pair, Biochemistry 43 (2004) 13787–13795.
[281] V. Petrouleas, D. Koulougliotis, N. Ioannidis, Trapping of metalloradical intermediates of the S-states at liquid helium temperatures. Overview of the phenomenology and mechanistic implications, Biochemistry 44 (2005) 6723–6728.
[282] K.G.V. Havelius, J. Sjöholm, F.M. Ho, F. Mamedov, S. Styring, Metalloradical EPR signals from the $Y_Z^\bullet$ S-state intermediates in photosystem II, Appl. Magn. Reson. 37 (2010) 151–176.
[283] H. Ishikita, B. Loll, J. Biesiadka, J. Kern, K.D. Irrgang, A. Zouni, W. Saenger, E.W. Knapp, Function of two β-carotenes near the D1 and D2 proteins in photosystem II dimers, Biochim. Biophys. Acta 1767 (2007) 79–87.
[284] J.L. Hughes, A.W. Rutherford, M. Sugiura, E. Krausz, Quantum efficiency distributions of photo-induced side-pathway donor oxidation at cryogenic temperature in photosystem II, Photosynth. Res. 98 (2008) 199–206.
[285] R. Gadjieva, F. Mamedov, G. Renger, S. Styring, Interconversion of low- and high-potential forms of cytochrome *b*559 in tris-washed photosystem II membranes under aerobic and anaerobic conditions, Biochemistry 38 (1999) 10578–10584.
[286] F. Mamedov, R. Gadjieva, S. Styring, Oxygen-induced changes in the redox state of the cytochrome *b*559 in photosystem II depend on the integrity of the Mn cluster, Physiol. Plant. 131 (2007) 41–49.
[287] E.M. Aro, I. Virgin, B. Andersson, Photoinhibition of photosystem II. Inactivation, protein damage and turnover, Biochim. Biophys. Acta 1143 (1993) 113–134.
[288] F. Mamedov, S. Styring, Logistics in the life cycle of photosystem II — lateral movement in the thylakoid membrane and activation of electron transfer, Physiol. Plant. 119 (2003) 328–336.
[289] R.K. Sinha, A. Tiwari, P. Pospisil, Water-splitting manganese complex controls light-induced redox changes of cytochrome $b_{559}$ in photosystem II, J. Bioenerg. Biomembr. 42 (2010) 337–344.
[290] J. Maroc, J. Garnier, Gel-electrophoresis of chloroplast membranes of mutants of *Chlamydomonas reinhardtii* which have impaired photosystem II function and lack photosynthetic cytochromes, Biochim. Biophys. Acta 637 (1981) 473–480.
[291] H.B. Pakrasi, P. Deciechi, J. Whitmarsh, Site directed mutagenesis of the heme axial ligands of cytochrome *b*559 affects the stability of the photosystem II complex, EMBO J. 10 (1991) 1619–1627.
[292] V.K. Shukla, G.E. Stanbekova, S.V. Shestakov, H.B. Pakrasi, The D1 protein of the photosystem II reaction centre complex accumulates in the absence of D2 — analysis of a mutant of the cyanobacterium *Synechocystis* sp. PCC 6803 lacking cytochrome *b*559, Mol. Microbiol. 6 (1992) 947–956.

[293] G. Ananyev, G. Renger, U. Wacker, V. Klimov, The photoproduction of superoxide radicals and the superoxide dismutase activity of photosystem II — the possible involvement of cytochrome *b*559, Photosynth. Res. 41 (1994) 327–338.
[294] A. Arató, N. Bondarava, A. Krieger-Liszkay, Production of reactive oxygen species in chloride- and calcium-depleted photosystem II and their involvement in photoinhibition, Biochim. Biophys. Acta 1608 (2004) 171–180.
[295] N. Bondarava, C.M. Gross, M. Mubarakshina, J.R. Golecki, G.N. Johnson, A. Krieger-Liszkay, Putative function of cytochrome *b*559 as a plastoquinol oxidase, Physiol. Plant. 138 (2010) 463–473.
[296] N. Mizusawa, T. Yamashita, M. Miyao, Restoration of the high-potential form of cytochrome *b*559 of photosystem II occurs via a two-step mechanism under illumination in the presence of manganese ions, Biochim. Biophys. Acta 1410 (1999) 273–286.
[297] M. Roncel, A. Boussac, J.L. Zurita, H. Bottin, M. Sugiura, D. Kirilovsky, J.M. Ortega, Redox properties of the photosystem II cytochromes *b*559 and *c*550 in the cyanobacterium *Thermosynechococcus elongatus*, J. Biol. Inorg. Chem. 8 (2003) 206–216.
[298] P. Pospisil, A. Tiwari, Differential mechanism of light-induced and oxygen-dependent restoration of the high-potential form of cytochrome *b*559 in tris-treated photosystem II membranes, Biochim. Biophys. Acta 1797 (2010) 451–456.
[299] P.M. Wood, The two redox potentials for oxygen reduction to superoxide, Trends Biochem. Sci. 12 (1987) 250–251.
[300] J. Komenda, J. Nickelsen, M. Tichy, O. Prasil, L.A. Eichacker, P.J. Nixon, The cyanobacterial homologue of HCF136/YCF48 is a component of an early photosystem II assembly complex and is important for both the efficient assembly and repair of photosystem II in *Synechocystis* sp. PCC 6803, J. Biol. Chem. 283 (2008) 22390–22399.
[301] J. Komenda, V. Reisinger, B.C. Müller, M. Dobáková, B. Granvogl, L.A. Eichacker, Accumulation of the D2 protein is a key regulatory step for assembly of the photosystem II reaction center complex in *Synechocystis* PCC 6803, J. Biol. Chem. 279 (2004) 48620–48629.
[302] M. Dobáková, M. Tichý, J. Komenda, Role of the PsbI protein in photosystem II assembly and repair in the cyanobacterium *Synechocystis* sp. PCC 6803, Plant Physiol. 145 (2007) 1681–1691.
[303] N. Adir, H. Zer, S. Shochat, I. Ohad, Photoinhibition — a historical perspective, Photosynth. Res. 76 (2003) 343–370.
[304] I. Vass, E. Aro, Photoinhibition of photosynthetic electron transport, in: G. Renger (Ed.), Primary Processes of Photosynthesis, Principles and Apparatus, RSC Publishing, Cambridge, U. K., 2008, pp. 393–425.
[305] A.K. Mattoo, J.B. Marder, M. Edelman, Dynamics of the photosystem II reaction center, Cell 56 (1989) 241–246.
[306] A.K. Mattoo, U. Pick, H. Hoffman-Falk, M. Edelman, The rapidly metabolized 32 000 dalton polypeptide of the chloroplast is the proteinaceous shield regulating photosystem II electron transport and mediating diuron herbicide sensitivity, Proc. Natl. Acad. Sci. U.S.A. 78 (1981) 1572–1576.
[307] G.F.W. Searle, A. Telfer, J. Barber, T.J. Schaafsma, Millisecond time-resolved EPR of the spin-polarized triplet in the isolated photosystem II reaction center, Biochim. Biophys. Acta 1016 (1990) 235–243.
[308] G.X. Chen, J. Kazimir, G.M. Cheniae, Photoinhibition of hydroxylamine-extracted photosystem II membranes — studies of the mechanism, Biochemistry 31 (1992) 11072–11083.
[309] I. Setlik, S.I. Allakhverdiev, L. Nedbal, E. Setlikova, V.V. Klimov, Three types of photosystem II photoinactivation. 1. Damaging processes on the acceptor side, Photosynth. Res. 23 (1990) 39–48.
[310] I. Vass, S. Styring, T. Hundal, A. Koivuniemi, E. Aro, B. Andersson, Reversible and irreversible intermediates during photoinhibition of photosystem II: stable reduced $Q_A$ species promote chlorophyll triplet formation, Proc. Natl. Acad. Sci. U.S.A. 89 (1992) 1408–1412.
[311] E. Hideg, C. Spetea, I. Vass, Singlet oxygen and free radical production during acceptor- and sonor-side-induced photoinhibition — studies with spin trapping EPR spectroscopy, Biochim. Biophys. Acta 1186 (1994) 143–152.
[312] E. Hideg, C. Spetea, I. Vass, Singlet oxygen production in thylakoid membranes during photoinhibition as detected by EPR spectroscopy, Photosynth. Res. 39 (1994) 191–199.
[313] N. Keren, A. Berg, P.J.M. van Kan, H. Levanon, I. Ohad, Mechanism of photosystem II photoinactivation and D1 protein degradation at low light: the role of back electron flow, Proc. Natl. Acad. Sci. U.S.A. 94 (1997) 1579–1584.
[314] S. Reinman, P. Mathis, Influence of temperature on photosystem II electron transfer reactions, Biochim. Biophys. Acta 635 (1981) 249–258.
[315] M. Volk, M. Gilbert, G. Rousseau, M. Richter, A. Ogrodnik, M.E. Michel-Beyerle, Similarity of primary radical pair recombination in photosystem II and bacterial reaction centers, FEBS Lett. 336 (1993) 357–362.
[316] K. Cser, I. Vass, Radiative and non-radiative charge recombination pathways in photosystem II studied by thermoluminescence and chlorophyll fluorescence in the cyanobacterium *Synechocystis* 6803, Biochim. Biophys. Acta 1767 (2007) 233–243.
[317] A. Koivuniemi, E. Swiezewska, E.M. Aro, S. Styring, B. Andersson, Reduced content of the quinone acceptor $Q_A$ in photosystem II complexes isolated from thylakoid membranes after prolonged photoinhibition under anaerobic conditions, FEBS Lett. 327 (1993) 343–346.
[318] I. Vass, K. Cser, Janus-faced charge recombinations in photosystem II photoinhibition, Trends Plant Sci. 14 (2009) 200–205.
[319] I. Vass, Role of charge recombination processes in photodamage and photoprotection of the photosystem II complex, Physiol. Plant. 142 (2011) 6–16.
[320] A. Gopher, Y. Blatt, M. Schonfeld, M.Y. Okamura, G. Feher, M. Montal, The effect of an applied electric field on the charge recombination kinetics in reaction centers reconstituted in planar lipid bilayers, Biophys. J. 48 (1985) 311–320.
[321] A. Krieger-Liszkay, A.W. Rutherford, Influence of herbicide binding on the redox potential of the quinone acceptor in photosystem II: relevance to photodamage and phytotoxicity, Biochemistry 37 (1998) 17339–17344.
[322] C. Gross, Entstehung von Singulettsauerstoff und Superoxid am Photosystem II, PhD thesis, Germany, University of Freiburg, 2008.
[323] A. Krieger, E. Weis, Energy-dependent quenching of chlorophyll *a* fluorescence — the involvement of proton-calcium exchange at photosystem II, Photosynthetica 27 (1992) 89–98.
[324] P.L. Dutton, J.S. Leigh, C.A. Wraight, Direct measurement of the midpoint potential of the primary electron acceptor in *Rhodopseudomonas spheroides in situ* and in the isolated state — some relationships with pH and o-phenanthroline, FEBS Lett. 36 (1973) 169–173.
[325] A. Trebst, Inhibitors in the functional dissection of the photosynthetic electron transport system, Photosynth. Res. 92 (2007) 217–224.
[326] W. Oettmeier, Herbicides of photosystem II, in: J. Barber (Ed.), Topics in Photosynthesis Vol. 11: The Photosystems: Structure, Function and Molecular Biology, Elsevier, Amsterdam, 1992, pp. 349–408.
[327] A. Trebst, The 3-dimensional structure of the herbicide binding niche on the reaction center polypeptides of photosystem II, Z. Naturforsch. C 42 (1987) 742–750.
[328] A. Takano, R. Takahashi, H. Suzuki, T. Noguchi, Herbicide effect on the hydrogen-bonding interaction of the primary quinone electron acceptor $Q_A$ in photosystem II as studied by Fourier transform infrared spectroscopy, Photosynth. Res. 98 (2008) 159–167.
[329] R. Takahashi, K. Hasegawa, A. Takano, T. Noguchi, Structures and binding sites of phenolic herbicides in the $Q_B$ pocket of photosystem II, Biochemistry 49 (2010) 5445–5454.
[330] D.J. Kyle, I. Ohad, C.J. Arntzen, Membrane protein damage and repair — selective loss of a quinone–protein function in chloroplast membranes, Proc. Natl. Acad. Sci. U.S.A. 81 (1984) 4070–4074.
[331] F. van der Bolt, W. Vermaas, Photoinactivation of photosystem II as studied with site-directed D2 mutants of the cyanobacterium *Synechocystis* sp. PCC 6803, Biochim. Biophys. Acta 1098 (1992) 247–254.
[332] H. Zer, I. Ohad, Photoinactivation of photosystem II induces changes in the photochemical reaction center II abolishing the regulatory role of the $Q_B$ site in the D1 protein degradation, Eur. J. Biochem. 231 (1995) 448–453.
[333] Y. Nakajima, S. Yoshida, T. Ono, Differential effects of urea/triazine-type and phenol-type photosystem II inhibitors on inactivation of the electron transport and degradation of the D1 protein during photoinhibition, Plant Cell Physiol. 37 (1996) 673–680.
[334] J. Komenda, J. Masojidek, The effect of Photosystem II inhibitors DCMU and BNT on the high-light induced D1 turnover in two cyanobacterial strains *Synechocystis* PCC 6803 and *Synechococcus* PCC 7942, Photosynth. Res. 57 (1998) 193–202.
[335] F. Rappaport, A. Cuni, L. Xiong, R. Sayre, J. Lavergne, Charge recombination and thermoluminescence in photosystem II, Biophys. J. 88 (2005) 1948–1958.
[336] J. Komenda, M. Koblizek, O. Prasil, Characterization of processes responsible for the distinct effect of herbicides DCMU and BNT on Photosystem II photoinactivation in cells of the cyanobacterium *Synechococcus* sp. PCC 7942, Photosynth. Res. 63 (2000) 135–144.
[337] C. Fufezan, F. Drepper, H.D. Juhnke, C.R.D. Lancaster, S. Un, A.W. Rutherford, A. Krieger-Liszkay, Herbicide-induced changes in charge recombination and redox potential of $Q_A$ in the T4 mutant of *Blastochloris viridis*, Biochemistry 44 (2005) 5931–5939.
[338] C. Fufezan, C.M. Gross, M. Sjödin, A.W. Rutherford, A. Krieger-Liszkay, D. Kirilovsky, Influence of the redox potential of the primary quinone electron acceptor on photoinhibition in photosystem II, J. Biol. Chem. 282 (2007) 12492–12502.
[339] S.A. Merry, P.J. Nixon, L.M. Barter, M. Schilstra, G. Porter, J. Barber, J.R. Durrant, D.R. Klug, Modulation of quantum yield of primary radical pair formation in photosystem II by site-directed mutagenesis affecting radical cations and anions, Biochemistry 37 (1998) 17439–17447.
[340] D.V. Vavilin, W.F. Vermaas, Mutations in the CD-loop region of the D2 protein in *Synechocystis* sp. PCC 6803 modify charge recombination pathways in photosystem II in vivo, Biochemistry 39 (2000) 14831–14838.
[341] S.S. Golden, Light-responsive gene expression in cyanobacteria, J. Bacteriol. 177 (1995) 1651–1654.
[342] B. Loll, M. Broser, P.B. Kos, J. Kern, J. Biesiadka, I. Vass, W. Saenger, A. Zouni, Modeling of variant copies of subunit D1 in the structure of photosystem II from *Thermosynechococcus elongatus*, Biol. Chem. 389 (2008) 609–617.
[343] P.B. Kós, Z. Deák, O. Cheregi, I. Vass, Differential regulation of *psbA* and *psbD* gene expression, and the role of the different D1 protein copies in the cyanobacterium *Thermosynechococcus elongatus* BP-1, Biochim. Biophys. Acta 1777 (2008) 74–83.
[344] D. Campbell, G. Zhou, P. Gustafsson, G. Oquist, A.K. Clarke, Electron transport regulates exchange of two forms of photosystem II D1 protein in the cyanobacterium *Synechococcus*, EMBO J. 14 (1995) 5457–5466.
[345] M. Tichy, L. Lupinkova, C. Sicora, I. Vass, S. Kuvikova, O. Prasil, J. Komenda, *Synechocystis* 6803 mutants expressing distinct forms of the Photosystem II D1 protein from *Synechococcus* 7942: relationship between the *psbA* coding region and sensitivity to visible and UV-B radiation, Biochim. Biophys. Acta 1605 (2003) 55–66.
[346] C.I. Sicora, S.E. Appleton, C.M. Brown, J. Chung, J. Chandler, A.M. Cockshutt, I. Vass, D.A. Campbell, Cyanobacterial *psbA* families in *Anabaena* and *Synechocystis* encode trace, constitutive and UVB-induced D1 isoforms, Biochim. Biophys. Acta 1757 (2006) 47–56.
[347] A. Krieger, A.W. Rutherford, Comparison of chloride-depleted and calcium-depleted PSII: the midpoint potential of $Q_A$ and susceptibility to photodamage, Biochim. Biophys. Acta 1319 (1997) 91–98.
[348] M. Broser, C. Glöckner, A. Gabdulkhakov, A. Guskov, J. Buchta, J. Kern, F. Müh, H. Dau, W. Saenger, A. Zouni, Structural basis of cyanobacterial photosystem II inhibition by the herbicide terbutryn, J. Biol. Chem. 286 (2011) 15964–15972.

[349] K. Kawakami, Y. Umena, N. Kamiya, J.R. Shen, Structure of the catalytic, inorganic core of oxygen-evolving photosystem II at 1.9 Å resolution, J. Photochem. Photobiol. B: Biol. 104 (2011) 9–18.
[350] J.R. Shen, Y. Inoue, Binding and functional properties of two new extrinsic components, cytochrome *c*-550 and a 12-kDa protein, in cyanobacterial photosystem II, Biochemistry 32 (1993) 1825–1832.
[351] J.R. Shen, N. Kamiya, Crystallization and the crystal properties of the oxygen-evolving photosystem II from *Synechococcus vulcanus*, Biochemistry 39 (2000) 14739–14744.
[352] M. le Maire, P. Champeil, J.V. Moller, Interaction of membrane proteins and lipids with solubilizing detergents, Biochim. Biophys. Acta 1508 (2000) 86–111.
[353] K. Kawakami, M. Iwai, M. Ikeuchi, N. Kamiya, J.R. Shen, Location of PsbY in oxygen-evolving photosystem II revealed by mutagenesis and X-ray crystallography, FEBS Lett. 581 (2007) 4983–4987.
[354] W. Humphrey, A. Dalke, K. Schulten, VMD: visual molecular dynamics, J. Mol. Graphics 14 (1996) 33–38.
[355] The PyMOL Molecular Graphics System, Schrödinger, LLC.